iScience

CellPress
OPEN ACCESS

Review

Two decades of two-photon lithography: Materials science perspective for additive manufacturing of 2D/3D nano-microstructures

Arun Jaiswal,[1,5] Chandresh Kumar Rastogi,[2,5] Sweta Rani,[3] Gaurav Pratap Singh,[1] Sumit Saxena,[1,3,4] and Shobha Shukla[1,3,4,*]

SUMMARY

Two-photon lithography (TPL) is a versatile technology for additive manufacturing of 2D and 3D micro/nanostructures with sub-wavelength resolved features. Recent advancement in laser technology has enabled the application of TPL fabricated structures in several fields such as microelectronics, photonics, optoelectronics, microfluidics, and plasmonic devices. However, the lack of two-photon polymerizable resins (TPPRs) induces bottleneck to the growth of TPL to its true potential, and hence continuous research efforts are focused on developing efficient TPPRs. In this article, we review the recent advancements in PI and TPPR formulation and the impact of process parameters on fabrication of 2D and 3D structures for specific applications. The fundamentals of TPL are described, followed by techniques used for achieving improved resolution and functional micro/nanostructures. Finally, a critical outlook and future prospects of TPPR formulation for specific applications are presented.

INTRODUCTION

Controlled fabrication of nano- and micro-scale features of desired structures and functionality is important for both fundamental research and applications. Advances in additive manufacturing technologies have enabled the fabrication of 2D and 3D micro/nanostructures with submicron resolutions and desired functional properties. Lithography-based fabrication techniques are extremely promising as they offer precise control over structural attributes including size, shape, resolution, and dimensions. Conventionally used lithographic techniques such as focused ion beam lithography (FIBL), electron beam lithography (EBL), nanoimprint lithography (NIL), and deep UV lithography (DUVL) can efficiently write the structures down to a few nanometers. However, these techniques have certain inherent drawbacks such as (1) complex instrumentation, (2) tedious fabrication process (step-by-step processing), (3) high vacuum requirements, and (4) harsh processing conditions. Besides, the ability of these techniques is largely limited for fabrication of 2D structures. These issues with the conventional lithographic techniques have led to the exploration of other microfabrication techniques.

In recent decades, two-photon lithography (TPL) has emerged as a promising technique that employs direct laser writing (DLW) for the fabrication of 3D nanostructures with high throughput and higher resolution for rapid prototyping. TPL relies on two-photon polymerization (TPP) process that involves sensitization of PI via two-photon excitation (TPE), and subsequent cross-linking of monomer/oligomer (polymerizable resin or photo-resist), using an intense pulsed laser beam. Though TPL is a very versatile and promising patterning technique for writing complicated 3D structures, it is not a scalable commercial technology yet because of the following drawbacks: (1) Low processing speed, (2) lack of commercial TPPRs, (3) low processing volume, (4) low dynamic range because of higher writing threshold, and (5) low two-photon absorption cross-section of TPPR.

Early studies on TPL claimed that the resolution (i.e., the linewidth and voxel dimension) critically depend on the process parameters, e.g., variation in numerical aperture, writing speed, average laser power, and exposure time.[1,2]. From a materials perspective, the feature size, shape, and resolution of TPL fabricated microstructures critically depend on the choice of the photoinitiator (PI), polymerizable resin or photoresist (PR). Special attention has been given in the past to design efficient PI and PR materials for TPP lithography.

[1]Nanostructures Engineering and Modeling Laboratory, Department of Metallurgical Engineering and Materials Science, Indian Institute of Technology Bombay, Mumbai, 400076, India

[2]Centre for Advanced Studies, Lucknow, 226031, India

[3]Nanostructures Engineering and Modeling Laboratory, Department of Metallurgical Engineering and Materials Science, Indian Institute of Technology Bombay-Monash Research Academy, Mumbai, 400076, India

[4]Water Innovation Center: Technology Research & Education, Department of Metallurgical Engineering and Materials Science, Indian Institute of Technology Bombay, Mumbai, MH 400076, India

[5]These authors contributed equally

*Correspondence: sshukla@iitb.ac.in

https://doi.org/10.1016/j.isci.2023.106374

This is an open access article under the CC BY license (http://creativecommons.org/licenses/by/4.0/).

The design strategy was centered on improving writing ability, i.e., exploring the possibility of fabricating microstructures with finer resolution at lower threshold power using two-photon excitation. Typically, a photoresist can be formulated using commercially available UV curable resins. The popular choices include acrylates (e.g., SCR500, pentaerythritol triacrylate (PETIA), and pentaerythritol tetraacrylate (PETA)) epoxies (e.g., SU-8), hydrogels (e.g., poly (ethylene glycol) diacrylate (PEGDA), N-isopropylacrylamide (NIPAM), and acrylamide), hybrid materials (e.g., Ormocer, OrmoComp, and SZ2080), and composite (e.g., PETA-Ni complex and methacrylic acid and titanium(IV) tetra-isopropoxide).

Very often, suitable dopants such as organic dyes (e.g., rhodamine B and methylene blue), carbon nanomaterials (CNTs), magnetic nanoparticles (Fe_3O_4), metallic salts (Au, Ag, and Ni) are introduced to photo-resist to induce additional properties that play a crucial role in the fabrication process and effective functionality of the developed structure. Sometimes, a sensitizer is also introduced to the PI (e.g., plasmonic NPs, fluorescent NPs or semiconductor QDs) to enhance the light absorption characteristics which results in radical formation and polymerization at lower threshold power. Verbitsky et al. formulated additive-free and solvent-free photoresist-based on quantum initiators. They used CdSe/CdS seeded nanorods as PIs for polymerization of hydroxyethyl acrylate and showed the use of these nanorods as efficient PIs as well as an efficient fluorescent probe.[3] Pawar et al. demonstrated the use of metal-semiconductor hybrid CdS-Au nanoparticles as a PI and achieved TPP fabrication without using any commercial two-photon initiator.[4] Unfortunately, the cytotoxicity because of the use of these nanoparticles restricts the use of these photoresists for biomedical applications. To mitigate this, use of molecules like curcumin has been explored as a PI to induce free radical polymerization of pentaerythritol triacrylate monomer resin.[5] Current research is devoted to the formulation of photo-resist and initiator with fewer chemical moieties. Though significant improvements in PR and PI formulations have been made in recent years, there is a renewed quest for the development of next generation of materials that require lower threshold power, higher resolution/precession and superior bio-compatibility.

In addition to innovation in materials designs and technical advancements in the fabrication process, the last decade has witnessed development in the area of modifying functionality and applications of microstructures. TPL fabricated nano/microstructures finds a plethora of potential applications in biomedical science (e.g., transdermal drug delivery,[6] cell growth studies, bio-degradable scaffold,[7] 3D DNA patterning[8]), design of optical components (e.g., microFresnel lens,[9] 3D optical micro-circuit,[10] and waveguide[11]), plasmonic devices (fiber-optic SERS probe[12]), electromechanical systems (NEMS, and MEMS[13]), and nano- and microfluidic.[14–27]

Although most of the reviews available in the literature have stressed on TPP-based additive manufacturing, a few of them have focused on commonly used materials for TPL.[28–31] Some of these reviews also include discussions on functional materials used in TPL targeting specific applications such as biomedical and therapeutic domains, photonics applications, stimuli-responsive structures and actuators.[32–44] Few others are based on a collection of fabrication strategies to improve the throughput and processing accuracy for achieving better resolution and build quality of the additively manufactured parts.[45,46] Thus, a wide scope is available for discussing the true aspects of TPL processing parameters and, material composition.

Here we have reviewed the most important milestones that have contributed significantly toward the development of this technology. We have emphasized on the recent developments in TPP-based microfabrication along with materials aspects (i.e., design of efficient two-photon absorbers and TPPRs) and optimization of TPL process parameters (i.e., laser fluence, fabrication speed, exposure duration) to obtain desired nano/microstructures. We begin with a review of the fundamentals of TPP fabrication techniques that cover the basic mechanism, experimental setup, and critical fabrication process parameters that influence the TPP. Various stages of TPL process for fabrication of high-resolution architectures with their applications are discussed. Finally, a brief outlook of challenges in the TPPRs formulation and possible methods to improve its characteristics are discussed with concluding remarks and future prospects.

FUNDAMENTALS OF TWO-PHOTON POLYMERIZATION

Two-photon absorption (TPA) is a non-linear optical process in which a fluorophore is excited to a higher state via a virtual intermediate state because of a sequential absorption of two photons of lower energy. To facilitate excitation by absorption of two photons, the sum of the energies of each isolated photon needs to match the electronic transition of the PI. Sometimes, a photosensitizer (PS) is introduced with

the PI to enhance its absorption characteristics. As the lifetime of the intermediate states of PS or PI is very small (~few femtoseconds), ultra-short laser pulses are required to realize TPA. This became possible only after the advent of ultrafast lasers. The TPL technique utilizes spatial confinement of TPA via a non-linear interaction of polymeric resin within the polymer matrix with tightly focused femtosecond laser pulses. Because TPA is confined to the area where light intensity is very high, it can induce photo-chemical and photo-physical changes, not only on the surface but also in the bulk of the material. TPL generally utilizes commercially available UV-curable photopolymers mixed with free radical or cationic PIs which absorb two photons of near-infra-red (NIR) light simultaneously and generate suitable species to initiate photo-polymerization. This leads to polymerized voxels (PV) with a volume of the order of femtoliters and hence features formed by TPL are of resolution beyond the diffraction limit. PV serves as the smallest building block for the microstructures, and smaller PVs allow the tighter arrangement resulting in better resolution and quality of the structures. For TPPR with higher TPP sensitivity, smaller PVs are formed as compared to the TPPR with low TPP sensitivity, furthermore, the PV size can be controlled by varying process parameters[47,48] and TPPR composition.[49] The lateral resolution of the fabricated lines (detailed derivation can be seen in theoretical section) can be expressed by the relation below[26];

$$w = r_0 \left[ln \left(\frac{\sigma \left(\frac{\eta \rho_0}{\rho_{th}} \right) \left(\frac{TP}{\hbar \omega_L} \right)^2}{\pi^{3/2} v_b \upsilon \tau_L r_0^3} \right) \right]^{1/2} \quad \text{(Equation 1)}$$

Where υ is the pulse repetition rate in MHz, v_b is scan speed in μm/s, τ_L is pulse width (in femtosecond), σ is the TPA cross-section of the PI, η is the two-photon quantum efficiency of the TPPR, r_0 is the laser beam waist radius, ρ_{th} is threshold photoacid concentration for initiation of polymerization, ρ_0 is the concentration of photoacid generated, T is the fraction of light transmitted through the microscope objective, and P is the average laser power to the microscope. So, from the above equation, it is evident that to achieve optimal resolution of TPPR composition and process parameters play a crucial role, and it depends on the excitation wavelength, excitation power, exposure time/scan speed, curability of the monomers in the resin, amount of quencher present in the resin and the TPA cross-section of the PI. The process parameters such as laser dosage and exposure time/(scan speed) can be easily controlled using components of TPL system, and the TPPR can be formulated to provide a large TPA cross-section.

The overall efficiency of TPP processes depends on the following three factors: (1) Two-photon absorption cross-section (σ) of PS, (2) PS → PI energy transfer efficiency, and (3) the quantum efficiency of the PI. This implies that there should be a good overlap in the electronic structure of PS and PI. For instance, the efficiency of a TPP process can be low, despite having a PS with a large TPA cross-section. This is possible if a large fraction of the absorbed energy is lost because of the low quantum yield of radical generation or intermolecular charge transfer between PI and PS. It has also been shown that PI with a low TPA cross-section and large quantum yield can be used to formulate a resin with sufficiently high TPP sensitivity.[49] For a photoresist with low TPP sensitivity, a higher average laser power is required for the initiation of the TPP processes that reduces the working window for TPL. An improvement in the TPP sensitivity can be achieved by the proper choice of TPPR. The material used as TPPR must display the following characteristics (1) high TPA cross-section, (2) high quantum yield of radical generation, (3) low fluorescent quantum yield, (4) rapid curability of monomers, (5) optical transparency to the writing wavelength, to avoid initiation of physio-chemical changes in the resin because of linear interaction, (6) good mechanical strength of the crosslinked chain to ensure that structures can withstand and retain original architecture during post-fabrication processing for the intended application.

TPL mechanism

TPP-based lithography, TPL comprises four processing steps[50], i.e., radical formation via TPA, initiation of cross-linking of monomer/oligomer, chain growth and termination of polymerization process as described by a scheme shown in Figure 1. During the TPA process sufficient energy is provided to PI molecule to initiate the TPP process by generating radicals from the PI molecules. The photo-generated radicals combine with monomers to form monomer radicals which act as active sites. These active sites sustain the chain reaction of previous events. This causes a progressive increment in the chain length until a monomer radical/radical combines with a growing chain, finally resulting in the formation of polymerized voxel (PV), i.e., the fundamental building block of the microstructures.

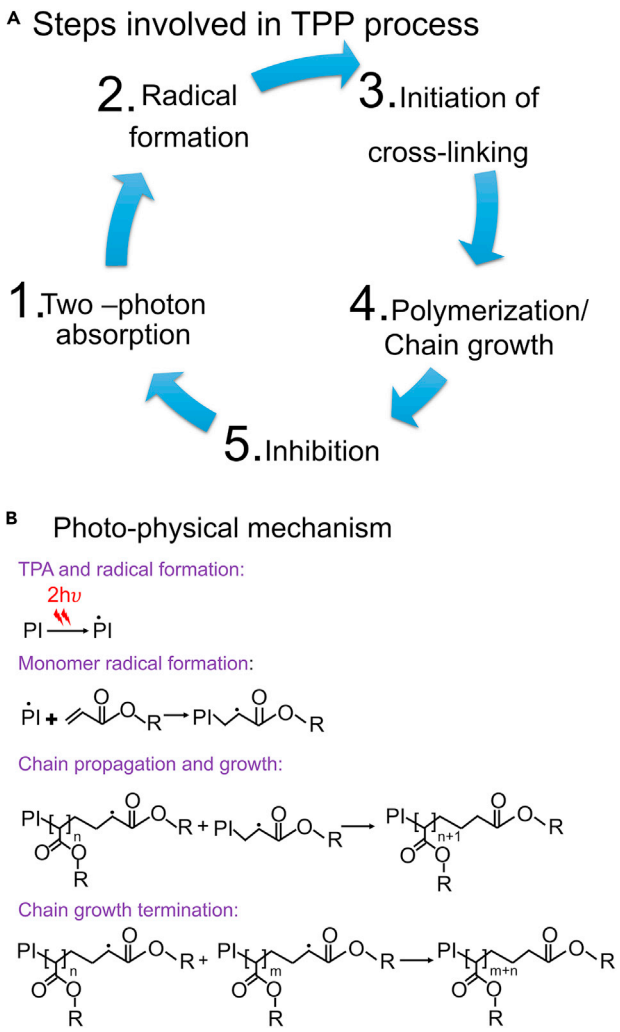

Figure 1. TPP mechanism

(A) Schematic depicting various steps involved in a TPP and (B) photo-physical/chemical mechanism occurring at each step.

TPL fabrication set-up

Various configurations of TPL printers have been reported in the literature; however, to attain TPP and subsequent fabrication, the essential functional components includes an excitation source and other optical units such as an ultrafast shutter (US) and a neutral density (ND) filter wheel, with high precision translation stage. A schematic of a TPL system is shown in Figure 2. Typically, a tunable femtosecond laser (operating in a working window 690–1040 nm; pulse width of 140 fs, and pulse repetition rate of 80 MHz) is used as an excitation source. Ti: Sapphire-based oscillators are considered ideal for TPL applications because they offer advantages in terms of a wide range of available wavelengths with ultra-short pulses, sufficing the need for high intensity and the temporal requirement for initiating two-photon processes.

The neutral density (ND) filter wheel is used to control the excitation power of the microscope. The beam is tightly focused into the TPPR using a large numerical aperture objective and the sample is scanned in three dimensions (3D) using a nanoprecision stage. TPL has been used for both negative as well as positive tone resins; however, negative tone resins are more popular for fabrication of nanostructures. Typically, for a negative tone resin, the unexposed resin is washed away using an appropriate developer whereas the fabricated structure remains adhered to the glass substrate. The microstructures mainly consist of densely packed polymerized voxels (PVs) with a small proportion of by-products generated during the radical

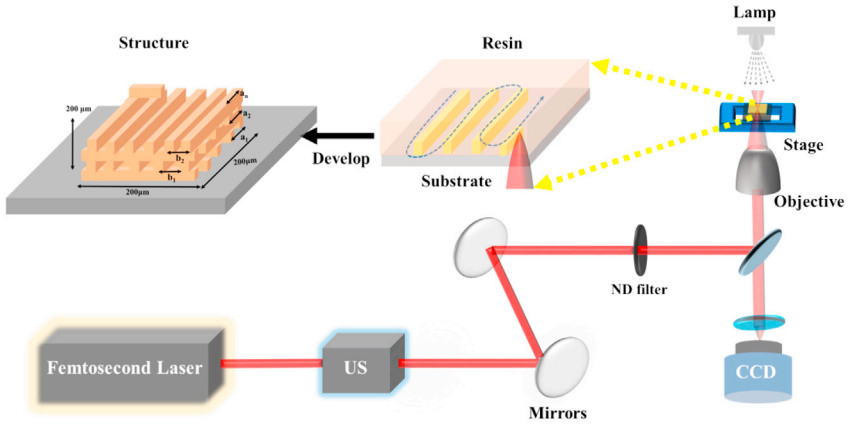

Figure 2. Schematic showing different components of TPL set up used for the fabrication of microstructure.

formation/photolysis of the PI/crosslinker. These PVs act as the basic building blocks for the additively manufactured structures using TPL, and define their resolution.

The minimal resolution is defined by the combination of material properties and processing parameters. Furthermore, the spatial resolution can be controlled with the proper selection of processing parameters, as the polymerized voxel resolutions are defined by the power above the writing thresholds. Sensitive resins offer lower writing thresholds and hence offer large processing windows. The spatial resolution can be controlled with the proper selection of processing parameters, as the polymerized voxel resolutions are defined by the power above the writing thresholds. TPL performed near the writing threshold provides the best resolution, and the voxel size tends to increase when the exposure power is kept well above the writing threshold as shown in Figure 3A. The power versus linewidth plot shown in Figure 3B, shows the increase of the lateral linewidth with an increase in average power. In addition, under identical experimental conditions, we can achieve controlled linewidths ranging from ~250 nm to ~1000 nm, simply by controlling the average laser power.

Based on the aforementioned facts, it can be summarized that to attain the best resolution one needs to opt for a system combining resin with high TPP sensitivity (providing a low writing threshold) and the optical parameters of the TPL printers should be selected to deliver best full-width half maxima (FWHM) to the sample. The two main factors limiting the resolution in TPL are:

1. Material system: The available TPPRs offer average to moderate TPP sensitivity, leading to the increased polymerization threshold. The increase of FWHM at the focal plane, with increased average laser power, can be associated with the reduced resolutions for the resins with higher writing threshold.
2. Optical components: Pulsed lasers when interact with the optical components of the TPL printer, several losses such as scattering, back reflection, absorption etc., are induced to the beam. The most critical parameter governing the FWHM of the laser pulses is the pulse-width which tends to broaden because of the group velocity dispersion (GVD) in the free air and the optical components such as guiding mirrors, filters, and polarizers. GVD induces pulse broadening, hence, altering the FWHM and the peak intensities available to the sample. For instance, Hann et al.,[53] reported an increase in the pulse duration by a factor of 10, whereas a 100 fs pulse traveled from the laser source to the focal plane. They used a prism-based arrangement for GVD compensation; however, the incorporation of additional components induces complexity to the optical path of the system and adds to the overall cost of the TPL printer.

Theoretical analysis

The resolution of TPP is highly correlated with the process parameters. This section discusses the crucial role of these parameters in the resolution of TPP using the models reported in the literature.[26,45] In our earlier report, we demonstrated a novel approach to design gold (Au) nanostructures embedded in a polymeric network with

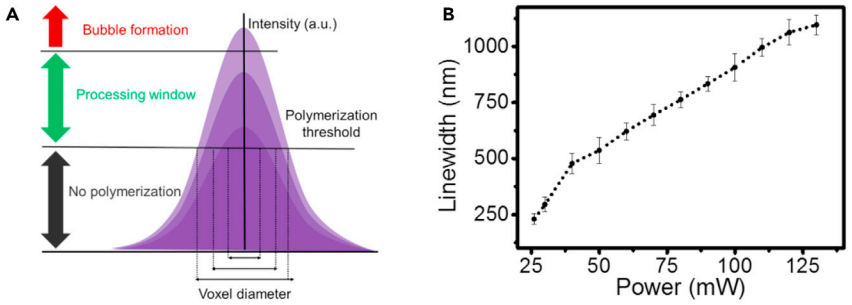

Figure 3. Threshold effect in TPP

(A) Radial distribution of the laser intensity at the focal plane[51] and (B) dependence of lateral resolution on the average laser power.[52] Reprinted (adapted) with permissions from IOP Publishing Group, ref.[51] and Elsevier, ref.[52].

sub-wavelength resolution.[26] The nanostructures were fabricated using Au-doped SU8 photoresist using a femtosecond pulsed laser. We implemented a first-order analytical model to estimate the linewidth (w) for the fabricated pattern. Explicit details of experimental conditions and fitting parameters can be found in our previous report.[26] In brief, to model the current system, we assumed that the photoresist (SU8) is polymerized at locations where the total photoacid generated (ρ) exceeds a threshold limit.

The density of radicals (ρ) produced by femtosecond laser pulses can be calculated by solving a simple rate equation.

If I is the photon flux intensity, then the density of radicals (ρ) produced by femtosecond laser pulses can be calculated by solving:

$$\frac{\delta\rho}{\delta t} = (\rho_0 - \rho)\sigma_2\eta I^2 \quad \text{(Equation 2)}$$

where I, $\rho_0\eta$, and σ_2 denote the photon flux intensity, primary initiator particle density, efficiency of the initiation process and the effective two-photon absorption coefficient of the dye employed for the sensitization, respectively.

Assuming that the initial density of radicals equals zero, the solution of the above equation can be expressed as:

$$\rho = \rho_0\left(1 - e^{-\sigma_2 I^2 t}\right) \quad \text{(Equation 3)}$$

where σ_2 is the effective two-photon cross-section for the generation of radicals, ρ_0 is the primary initiator particle density and I is the photon flux intensity.

Assuming that photon flux has a Gaussian spatial distribution and is constant (N_o) during each pulse of duration τ_L the polymerized linewidth (w) is given by

$$w = r_0\left[ln\frac{\sqrt{\pi}\sigma_2 n\upsilon\tau_L r_0 N_0^{2^{1/2}}}{2v_b C}\right] \quad \text{(Equation 4)}$$

where,

$$C = \ln(\rho_0/\rho_0 - \rho_{th}) \quad \text{(Equation 5)}$$

To evaluate "w" one can relate photon flux to the average laser power

$$N_0 = \frac{2}{\pi r_0^2 \upsilon\tau_L}\frac{TP}{\hbar\omega_L} \quad \text{(Equation 6)}$$

The overall expression for linewidth can be written as

$$w = r_0 \left[ln \frac{\sigma_2 \eta \left(\frac{TP}{\hbar\omega_L}\right)^2}{\pi^{3/2} v_b \upsilon \tau_L r_0^3 \ln\left(\frac{\rho_0}{\rho_0 - \rho_{th}}\right)} \right]^{1/2} \quad \text{(Equation 7)}$$

In case $\rho_{Th} \ll \rho_0$

Then,

$$w = r_0 \left[ln \left(\frac{\sigma_2 \frac{\eta \rho_0}{\rho_{th}} \left(\frac{TP}{\hbar\omega_L}\right)^2}{\pi^{3/2} v_b \upsilon \tau_L r_0^3} \right) \right]^{1/2} \quad \text{(Equation 8)}$$

The above equation was used to fit the experimental and the calculated linewidth "w" as a function of average laser power P both in the presence and absence of the gold precursor.[26] The findings are shown in Figure 4A. The experimental data used for the fitting model is tabulated in Table 1 below.

The expression for voxel diameter as a function of average laser power (P), pulse width (τ), beam waist (ω_0), and effective TPA cross-section is derived as follows. Considering the Gaussian nature of incident beam, distribution of photon flux intensity I(r, z) at distances of r along the cross section and of z in the propagation direction from the center can be expressed as:

$$I(r,z) = I_0 \left(\frac{\omega_0^2}{\omega_z^2}\right) e^{\frac{-2r^2}{\omega_z^2}} \quad \text{(Equation 9)}$$

where I_0, ω_0 and $\omega(z)$ are the photon flux intensity at beam center (r = 0, z = 0), beam waist, and beam radius in the plane at a distance z, respectively.

Where ω_0 and $\omega(z)$ can be expressed as follows:

$$\omega_0 = \frac{\lambda}{\pi NA} \sqrt{n_{oil}^2 - NA^2} \quad \text{(Equation 10)}$$

$$\omega(z) = \omega_0 \sqrt{1 + \left(\frac{\lambda z}{\pi \omega_0^2}\right)^2} \quad \text{(Equation 11)}$$

Where NA, λ and, n_{oil} denote numerical aperture of the objective lens, wavelength of laser beam, and the refractive index of immersion oil, respectively.

Neglecting the losses of radicals between the laser pulses, the voxel diameter can be correlated with average laser power (P), pulse width (τ), beam waist (ω_0), and effective TPA cross-section (σ_2) as follows:

$$d(P,t) = \omega_0 \left(\ln \frac{\sigma_2 I_0^2 f t \tau}{C} \right)^{1/2} \quad \text{(Equation 12)}$$

The variation of voxel diameter as a function of exposure time, average laser power, and numerical aperture (NA) of the objective is shown in Figures 4D and 4E. The increase in average laser power resulted in a slimmer voxel than increasing exposure time which is attributed to focal spot duplication law and voxel growth law. A model validating focal spot duplication law and voxel growth law in shown in Figures 4B and 4C. The details of the fitting parameters used are provided in Table 1.[45]

Approaches such as sub-regional slicing method (SSM),[10] parallel lithography,[11] autofocusing and simultaneous spatiotemporal focusing (SSTF) of the femtosecond laser (SSTF-TPP),[12] femtosecond projection TPL (FP-TPL) techniques[13] have been used to fabricate nanostructures with high throughput and greater resolution for rapid prototyping. Factors that greatly influence the resolution of fabricated microstructures are laser parameters (pulse width, intensity), optical parameters such as numerical aperture of the

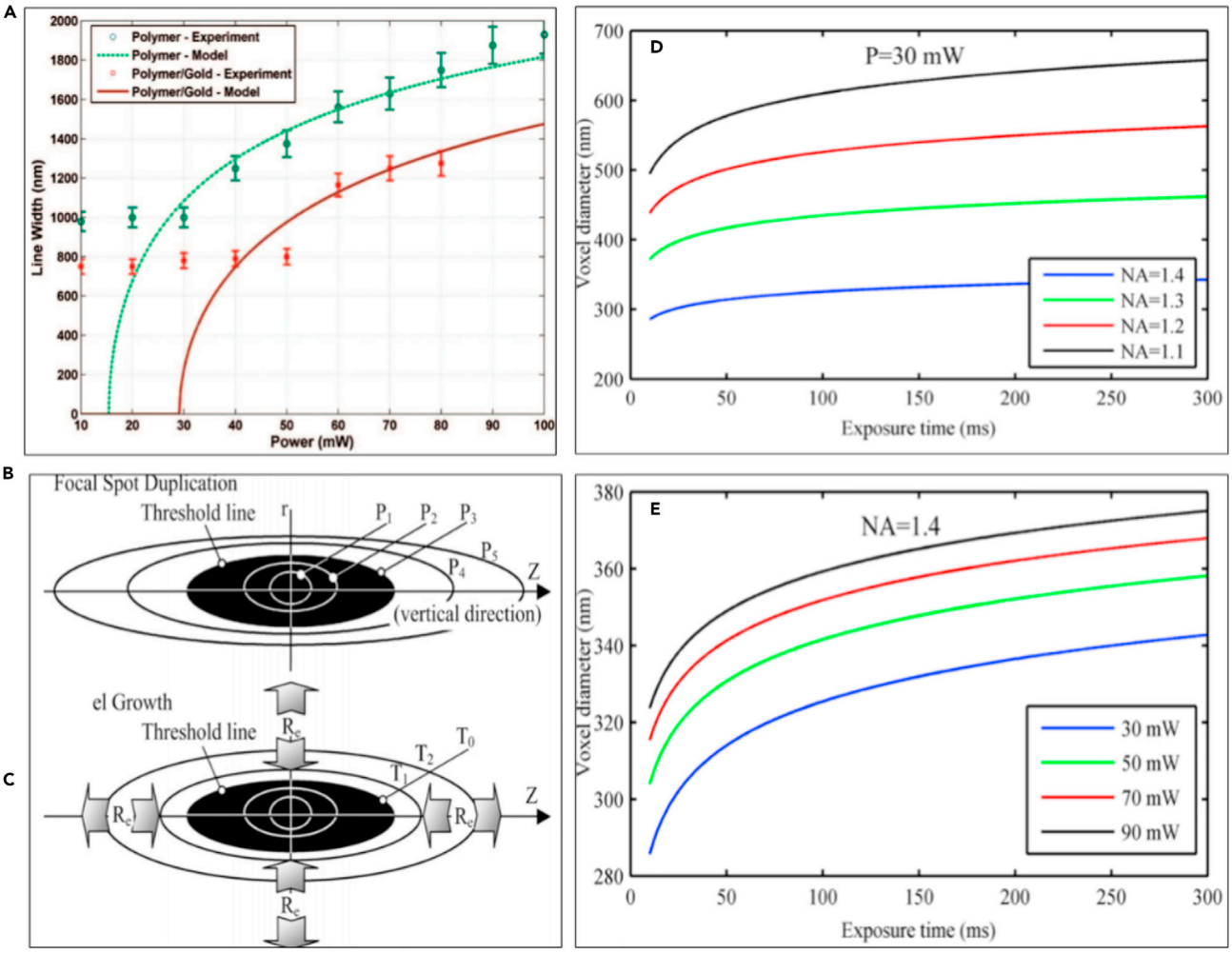

Figure 4. Effect of process parameters and focusing optics on fabrication resolution

(A) Polymerization line width versus average laser power: comparison of model with experimental data (Fitting parameters: r_0 = 940 nm, T = 30%, and $\eta\rho_0/\rho_{Th}$ = 0.0028 and 0.01 for polymerization with and without the gold precursor, respectively, models for initial voxels formation and growth (B) focal spot duplication and (C) voxel growth, variation of voxel diameter as a function of exposure time for (D) varying numerical aperture, and (E) varying power. Reprinted (adapted) with permission American Chemical Society, ref. [26] and AIP Publishing, ref. [45].

focusing objective, threshold power, TPP sensitivity, optical planarity of the substrate, and TPP sensitivity. The correlation of the processing parameters, material composition and the optical components of the TPL system critically controls the resolution and the build quality of the final constructs.

ADVANTAGES AND LIMITATIONS OF TPP TECHNIQUE

TPP uses a pulsed laser system that operates in the near infra-red region, where most of the curable monomers and polymers are transparent. This enables the laser light to penetrate deeper. Besides, TPA occurs only in defined spatial regions where the light intensity is high enough. Owing to this feature, this process can polymerize a small and specific region in the bulk of the liquid resin, without making any changes to its surface or the surrounding region. TPP-based microfabrication has a set of unique advantages such as (1) fabrication of high-resolution micro/nanostructures with greater precision, (2) 3D printing in a single exposure step and (3) fabrication of complex features with high accuracy and repeatability over conventional microfabrication techniques.

Unfortunately, the raster scanning of tiny voxels results in longer printing time which makes this method unsuitable for mass production. A few developments have been made for parallel processing, to achieve

Table 1. Values of process parameters used for numerical analysis as reported in ref[26,45]

S.No.	Parameter value	Ref.[26]	Ref.[45]
1	Wavelength of laser beam, λ(nm)	800	780
2	Laser pulse width, τ (fs)	120	100
3	Laser repetition frequency, f (MHz)	76	80
4	Two-photon cross-section, σ^2 (cm^4s)	3×10^{-49}	3×10^{-55}
5	Writing speed, v (μms^{-1})	50	–
6	Primary initiator particle density, ρ_0	–	2.4%
7	Threshold radicals density, ρth	–	0.25%
8	Planck constant, h (J.s)	–	$6.62606896 \times 10^{-34}$
9	Speed of light in vacuum, c (m/s)	–	3×10^8

improved throughput.[53–55] However, the overall processable volume is restricted to the microvolumes offered by the large numerical aperture of the focusing optics. In addition, the average power of the femtosecond pulsed lasers are expensive commodity, hence limiting the number of spots that can be processed at once. Besides, availability of limited photoresists forms a bottleneck. For example, the currently available photo-resists are not suitable for designing scaffolds that can mimic the native extracellular matrix (ECM) of human tissues because of lack of mechanical strength.[56] In addition, production of a microstructure composed of more than one material is a tedious process requiring multiple printing steps with intermediate processing procedures.

Microstructure fabrication

Microstructures-like woodpiles, scaffolds, nanowires, nanopillar arrays and other hierarchical structures have been fabricated using TPL. Kawata et al. demonstrated the fabrication of structures with a sub-diffracted resolution of ~120 nm using acrylic resin.[48] It was also reported that the fabrication process parameters (e.g., variation in numerical aperture, writing speed, average laser power, and exposure time) critically influence the linewidth and voxel dimension.[1,2]. Juodkazis reported the fabrication of nanorods with a lateral resolution of 30 nm using SU-8 photoresist.[57] Ultrafine nanofibers of diameter ~23 nm were fabricated using an approach of re-polymerization of lower degree polymerized structure of SCR500 resin. The SEM image of nanofiber is shown in Figure 5A. The feature size drastically decreases with scan speed as shown in Figure 5B. Tan et al. (2007) were able to reduce the feature size up to 15 nm using SCR500 photoresist by re-polymerization between two structures.[58]

Recent reports have focused on fabrication of bulk 3D structures with high throughput, greater precision, and minimal post-exposure processing, in addition to investigating their functional characteristics for intended applications. DPHPA-based monomers (dipentaerythritol penta/hexaacrylate) were used to directly write complex defect structures in holographically formed 3D photonic crystals. The SEM image of defect line in 3D photonic crystal template, and a structure generated by five beam interference pattern is shown in Figures 5C and 5D, respectively. Recently, autofocusing and SSTF of the femtosecond laser (SSTF-TPP) were used to fabricate bulk 3D structures with greater precision.[62] Applying SSTF approach on TPL technique, Chu et al. demonstrated a novel method to design centimeter-height 3D structures with an isotropic spatial resolution of 10–40 μm that could be tuned by simply varying the power of femtosecond laser, Figure 5E.[62] Park et al. (2005) introduced a nanostereolithography (NSL) based TPL technique to fabricate nanostructures with high throughput.[59] This method relies on sub-regional slicing method (SSM) and is efficient for quick writing of the nanostructure. The SEM image of a microjar fabricated using this method is shown in Figures 5F–5I. Later, Jeon et al. introduced a parallel lithographic technique by using a mask in a conventional TPP based lithography to form complex structures of controlled shape with improved resolution.[60] Haskeet al. used 4,4′-bis(di-*n*-butylamino) biphenyl chromophore to initiate crosslinking in a triacrylate blend and reported the fabrication of a structure with a feature size of ~65 nm[61]

Recently, Sahaet et al. developed a femtosecond projection TPL (FP-TPL) technique to realize simultaneous spatial and temporal focusing of ultrafast light and achieve parallel printing of arbitrarily complex 3D structures with submicrometer resolution.[63] These approaches appear to be extremely flexible and easy to

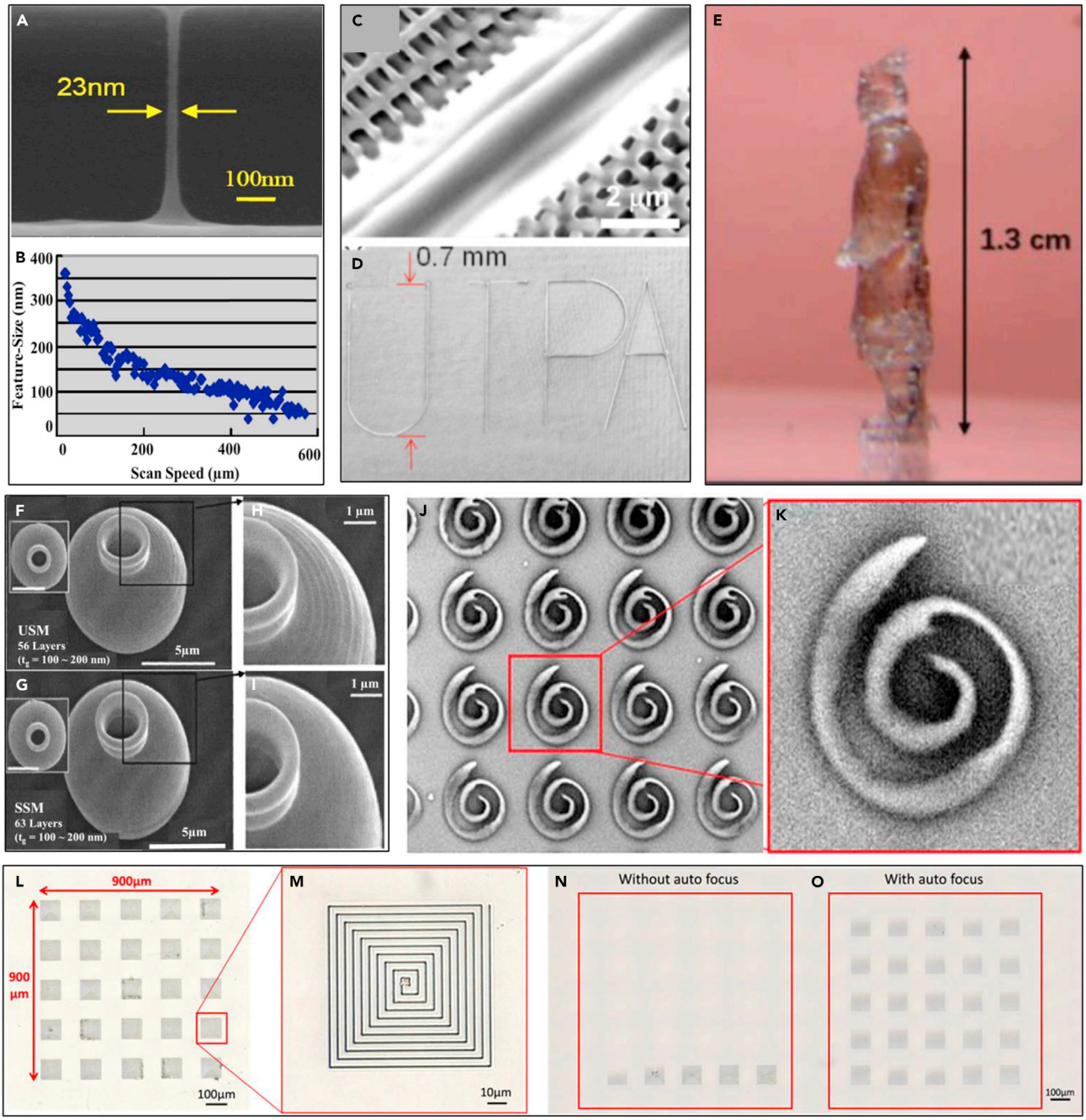

Figure 5. Various microstructures fabricated using TPL

(A) SEM images of nanofibers,[58] (B) Power versus linewidth plot,[58] SEM images of (C) Periodic 3D photonic crystal,[64] (D) Image of a five-beam interference pattern, (E) Chinese ornament (Terracotta warrior) with a height of 1.3 cm 3D structures achievable with SSTF-TPP,[62] (F), Microjars[59] (G–I). (J and K) micro-spiral structures,[63] Optical microscope images of (L–N) microstructure arrays fabricated with and (O) without auto-focusing technique.[65] "Reprinted (adapted) with permissions ref. 58,[64] and,[59] AIP Publishing, ref.[62], John Wiley & Sons, Inc., ref.[63], Science magazine, and ref.[65] Optica Publishing Group.

implement for designing of bulk 3D structures. Maruo et al. introduced a simple autofocusing technique in TPL by image processing of transmission images of photopolymerized voxels. The microstructure arrays with and without autofocusing are shown in Figures 5L–5O.

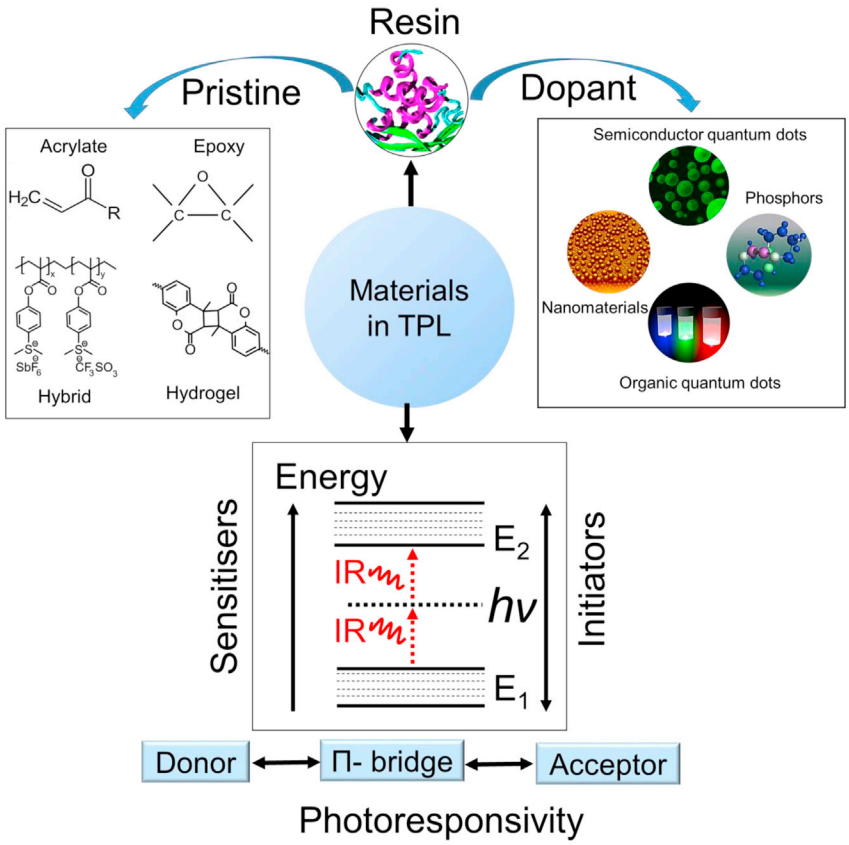

Figure 6. Schematic showing classification of different materials used in TPL; resins, PIs and PSs, based on their composition, characteristics, and performance.

Materials design

The feature size, shape and resolution of TPL fabricated nano/micro-architectures strongly depend on the choice of PI, polymerizable resin (PR), and writing parameters. Special attention has been given in past to design materials that can serve as efficient PI and PR for TPP. This section reviews the most widely reported materials used to date. The materials used in TPL can be classified into four groups, namely, polymerizable resin or photo-resist, PI, photosensitizer PS, and dopants. These are further categorized into different types of PR, PI, PS, and IT, based on their composition, performance, and properties. The chart in Figure 6, shows different classes of photoresist, dopants, and sensitizer materials.

Two-photon polymerizable resin (TPPR)

The most versatile approach to design a functional TPPR involves the incorporation of suitable dopant species (e.g., metal/carbon nanoparticles, dyes, semiconductor quantum dots, biomolecules), to impart additional functional characteristics to the micro/nanostructures. In general, TPPRs are multi-component systems, prepared by mixing different compatible molecules (e.g., photosensitive monomers, oligomers, initiators/inhibitors and/or sensitizers) in a predetermined proportion, with each component having a particular role in TPP. The role of TPPRs in TPL process is analogous to that of UV curable photo-resists in UV lithography, the only difference being it gets sensitized via a TPA process rather than a single photon excitation. The monomers/oligomers in TPPR get polymerized via cross-linking on exposure to the radiation of suitable energy. The polymerization process is terminated once the inhibitor interacts with cross-linking radical.

Different components of TPPRs and the fundamental mechanism of TPP have already been described above. Typically, TPPRs can be formulated using commercially available UV-curable resins. Popular choices include acrylates, epoxies and oligomers (owing to their rapid curing properties and ease of incorporating

Table 2. List of the widely used monomers and PI, processing parameters and functionality of nano/microstructures fabricated using TPP

Resin	Resin Name	Photoinitiator	Power[a] (mW)	Speed[b] (μm/s)	Resolution (nm)	Proposed Functionality	Reference
Epoxy	SU-8-2075	SU-8-2075	1.5–6	300	10,000	Fabricate Bulk Structure	62
Acrylate	BADGE	–	50–40	100–1000		Waveguide	82
	DDA + DPPHA	BDEBP and ITX	0.10	40	80	Woodpile	70
	PETIA	Lucirin TPO-L, curcumin	–	–	–	μ-structure to entrap and kill *Staphylococcus aureus* bacteria	5
	IP-Dip	IP-Dip	10–33	–	184	Diffraction Grating	81
	TMSPMA	DETC	20	2000		Biomedical	83
	SR368, SR499	L-TPO-L	18	–		Plasmonic Grating	27
	IP-Dip	IP-Dip	10	500	500	Large-scale nano proto-typing	82
	IP-Dip and IPL	–	33.6	25000	–	AFM Tip	84
	SCR500	–	20			First paper on TPP	50
	IPL-780	IPL-780	4	30	300	Drug screening	85
	IP-S	IP-S	–	–		Piezoelectric micro-bot	75
	PEGDA	2,7-bis(2-(4-pentaneoxy-phenyl)-vinyl)-anthraquinone (N)	3.8–7.7	110	–	Cell Scaffold	86
Hydrogel	DMAA-co-AAHAQ	–	25	10000	–	Protein Repellency Test	87
	Methacrylate gelatin	PEGDA + Benzylidenecycloketone	65	60–150	–	Human BJ cell line	73

BADGE: bisphenol-A diglycidylether, TMSPMA: 3-(trimethoxysilyl)propyl methacrylate, BDEBP: 4,4′-bis(diethylamino)benzophenone, ITX: isopropyl thioxanthone, PI- Photoinitiator, PS- Photosensitizer, CL-cross-linker, TMPTA: trimethylopropane triacrylate; PETIA: pentaerythritol triacrylate, DPHPA-dipentaerythritol-pentaacrylate; NPVP- N-vinyl pyrrolidinone.

[a]Laser writing power.

[b]scan speed.

foreign species). Very often, suitable dopants such as fluorescent species (e.g., quantum dots, dyes and luminescent inorganic nanoparticles[66]), carbon nanomaterials (nanotubes[67] and carbon quantum dots), magnetic nanoparticles (Fe_3O_4), metallic nanoparticles (Ag, Au, and Ni)[68] are introduced to TPPRs to induce additional functionality in the fabricated microstructure.[15,16] It is advisable to design a TPPR with a minimal number of constituents as a multi-component system can hamper the polymerization processes.[69]

TPPRs can be categorized as positive tone or negative tone photoresists depending on PI/inhibitor composition in the resin formulation. Here, we emphasize on negative TPPRs as they are commonly used for TPP fabrications. They also offer remarkable properties such as better resolution, shape accuracy, excellent capabilities to adhere various substrates and optimal mechanical stability. A brief discussion about positive TPPR is given toward the end of this section.

In the past, a wide range of negative TPPRs has been formulated to fabricate microstructures that find applications in photonic and mechanical metamaterials, diffractive optical elements, mechanical components, cell scaffolds and microfluidics, to name a few. The most widely used negative TPPRs are epoxies, acrylates, hydrogels, and organic-inorganic hybrid materials. This review investigates only popular or recently developed TPPRs. In this series, we have classified them based on composition and functionality (Figure 6). The details of a few popular epoxies, acrylate and hydrogel-based resins used in two-photon lithography are given in Table 2, whereas the information related to hybrid material and composite resins is provided in Table 3. The details of the processing parameters, resolution of fabricated structure, and the proposed functionality are also mentioned in the same table. The molecular structure of a few of them is shown in Figure 7.

Table 3. List of the widely used hybrid monomers and photoinitiator, processing parameters and functionality of nano/microstructures fabricated using TPP

Resin	Name	Photoinitiator	Power[a] (mW)	Speed[b] (μm/s)	Resolution (nm)	Proposed Functionality	Reference
Hybrid	PETA + Ni based complex)	7-diethylamino-3-thenoylcoumarin	17.5–22.5	4 000- 6000	25–100	3D MEMS	72
	SZ2080	SZ2080	11.5	15	1000	Cell migration and separation	89
	Ormocer	–	–	–	100	Woodpile structure for photonic Application	18
	Ormocer	–	0.1 (J/cm^2)	750	500	3 PP	18
	Ormocomp	–	10	50	482	Axon mechanobiology	90
Composite	PETA + Ni based complex)	7-diethylamino-3-thenoylcoumarin	17.5–22.5	4 000- 6000	25–100	3D MEMS	72
	PETA + QDs (CdSe/CdS/ZnS)	Irgacure-819	8	100	75	Nanoemitter	91
	PEGDA + NIPAM + Fe_3O_4 NPs	Benzil (PI) + 2-benyl-2-(dimethylamino)-4′ -morpholinobutyrophe-none (PS)	0.48–4.4	6	200 nm	Actuator	16
	Methacrylic acid and titanium(IV) tetraisopropoxide (C12H28O4Ti)	DABD	10–16.5	Exposure time 10 (ms)	650	Microsized pressure sensor	74
	Ormocomp/$BaTiO_3$NPs		30	50		Cell Simulation	92

PI- Photoinitiator, PS- Photosensitizer, 3 PP: Three photon polymerisation, CL-cross-linker, PETA: pentaerythritol tetraacrylate, DABD, MP- 1-[4-(methylthio) phenyl]-2-methyl-2-morpholinopropan-1-one, AF 83 ∼6-benzothiazol-2-yl∼2-naphtyl diphenylamine; DPHPA-dipentaerythritolpentaacrylate.
[a]Laser writing power.
[b]Scan speed.

Epoxy

SU-8, an epoxy-based material, is one of the most commonly used negative photoresists for micro/nano-fabrication. Kim et al. used TPL technique to fabricate SU-8 based magnetic micro-bristle-bots and micro-robots of cylindrical and hexahedral shapes.[75] They functionalized the microrobots by coating them with a layer of Nickel (Ni) and Titanium (Ti). The Ni layer provided magnetization and enabled the control of the microrobots with external magnetic fields, whereas the Ti layer was used as a biocompatible material which enhanced the affinity with the cells. In general, it is extremely difficult to fabricate structures with heights beyond few hundred micrometers using TPL because of the limited working distance range provided by the microscopic objectives. There is a trade-off between the resolution of fabrication and the dimension of the final architecture. The complicated 3D architectures can be prepared at the expense of resolution. To fabricate the structures with large heights, Chu et al. demonstrated the use of simultaneous spatiotemporal focusing of laser pulses to write the bulk structure with a height of 1.3 cm using SU-8 resin.[62]

Acrylate

The first reported work on TPL[50] utilized acrylate-based resin (e.g., SCR500) for the manufacturing of a 3D microstructure. Since then, a variety of acrylate-based TPPRs have been used for fabrication of high-resolution micro/nanostructures applicable in various domains including MEMS, photonics and biomedical among others. Baldacchini et al. used ethoxylated (6) trimethylolpropane triacrylate and tris (2-hydroxyethyl) isocyanurate triacrylate photo-resist to fabricate 3D structures with high aspect ratio and intricate details.[76,77] The structure demonstrated good mechanical strength and high structural rigidity, suggesting suitability of acrylates to manufacture microstructures. Zandirini et al. studied the effect of resin viscosity on the resolution and the mechanical integrity of the structure for four different acrylate formulations prepared using acrylate-based resins DPEPA and BGDA.[78] They inferred that low viscosity of TPPRs resulted in the creation of higher-resolution structures.

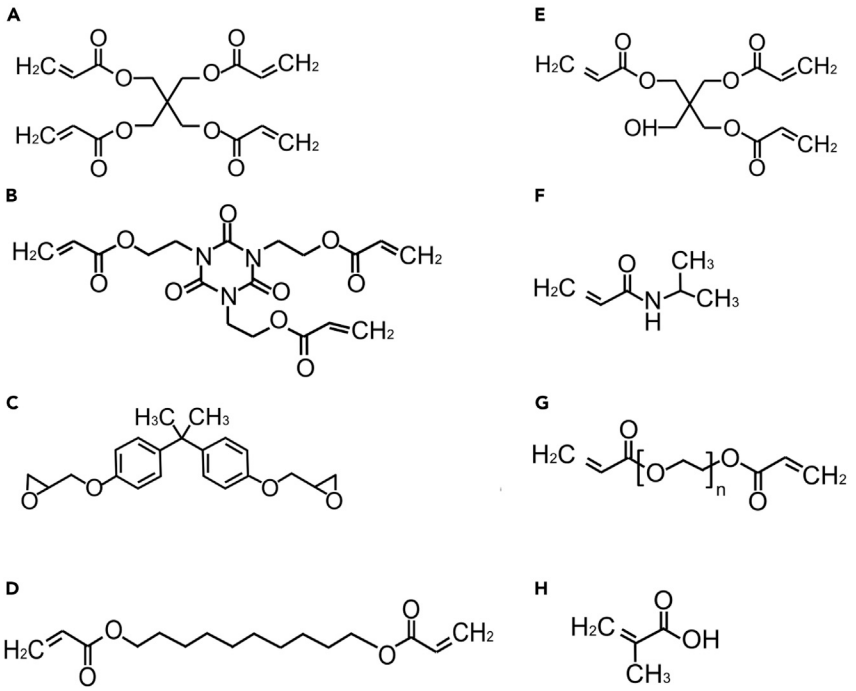

Figure 7. The chemical structures of popular resins used in two-photon lithography

(A) DPPHA Dipentaerythritol penta-/hexa-acrylate.[70] (B) tris (2-hydroxy ethyl) isocyanurate triacrylate,[27] (C) bisphenol-A diglycidylether,[71] (D). DDA 1,10-decanediol diacrylate,[70] (E). PETA,[72] (F). NIPAM,[16] (G). PEGDA[73] and (H). MMA.[74].

The other popular acrylate photo-resist used in TPP fabrication belongs to IP-series e.g., IP-L, IP-S and IP-Dip, however, these IP-series resists are proprietary, and are not readily available. Alexander et al. reported the fabrication of an IP-Dip photoresist-based implantable micro-caged device which could be used for controlled delivery of therapeutic agents at local sites. They reported that the drugs can be encapsulated into a needle-sized porous device and delivered in a controlled manner to the targeted tissues.[79] Berwind et al. demonstrated the fabrication of hydrophilic/hydrophobic biocompatible surfaces, using IP-Dip photoresist.[80] Purtov et al. demonstrated fabrication of nanopillar diffraction gratings with varying pillar sizes in IP-Dip resin.[81] The variation in the dimensions of the nanopillar gratings resulted in variation in the reflection obtained from the structure. The grating element dimensions were kept below 200 nm, to obtain the response in the visible region and the variation of grating element dimensions resulted in variation in their optical appearance. Various composites of IP-S photoresist have also been used in applications such as fabrication of sensors and electrodes.[29]

Hydrogels

Hydrogels are 3D network of cross-linked polymer chains with the ability to retain large amounts of water. Owing to the presence of a large number of functional groups at the surface of hydrogels, surface engineering of hydrogels with a suitable functional group is possible. The surface functionalized hydrogels exhibit good response to external stimuli and are suitable for fabrication of stimuli-responsive micro/nano-devices. Brigo et al. used gelatin-based woodpile for cell viability studies and reported that the exact amount of cell adhesion and invasion was dependent on the degree of polymerization of hydrogels in the scaffold.[73] Mechanical strength of structure and porosity are crucial parameters for tissue/cell culture applications. In this direction, Guo et al. were able to obtain structures with Young's modulus varying in the range (3.50–6.52) MPa.[86] Such controlled mechanical strength can be useful in designing cell scaffolds for cartilage repair.

A hydrogel containing an acetylacetone group was used as the photoactive system, which was prepared by polymerization of acryloyl acetone, acrylamide and N,N′-Methylene-bis-acrylamide. This demonstration of irreversible actuation of a cantilever deflection opened up the possibility of fabrication of movable 3D micromachine components and microfluidic systems which can be controlled optically.[15] An efficient

photopolymerizable hydrogel precursor was prepared by dissolving monomer acrylamide and co-monomer AMPS with cross-linker methylene-bis-acrylamide, PI benzil and PS 2-benzyl-2-(dimethylamino)-4′-morpholinobutyrophenone in a hydrophilic solvent consisting of a mixture of methanol, DMSO and glycerol. A microcantilever was fabricated in this hydrogel by using asymmetric 3D MPP technique and it was found that controlled bending could be achieved in water medium, and that the bending direction could be reversed by using an aqueous solution of NaCl. Because the water content of hydrogels is similar to that of the soft tissues and they can mimic the chemical, biological, and mechanical properties of native tissues, therefore hydrogels are widely employed in scaffold fabrication for tissue engineering and drug delivery. Hyaluronic acid (HA), being a major component of human extracellular matrix, has been exploited for fabrication of scaffolds for tissue engineering. Kufelt et al. demonstrated the fabrication of scaffolds in HA-based materials via TPP.[88] Photopolymerisable HA was produced by using glycidal methacrylate-based modification, which resulted in the formation of hyaluronic acid-glycidylmethacrylate (HAGM). Although the HA-backbone can promote controlled cell arrangement and guide tissue formation by providing important binding sites for cell arrangement, however, the mechanical properties were very poor. It was found that the increased mechanical load capacity could be achieved by polymerisation of HAGM, as compared to the typical viscoelastic gels. Furthermore, it was also demonstrated that the mechanochemical properties could be tailored by combining and crosslinking HA covalently with PEGDA. Different ratios of PEGDA could be added to HA for modulating the mechanical properties without affecting biocompatibility. Fabrication of complex 3D scaffolds with tailored properties by using TPP promises prospects for investigation of cell behavior in a reproducible 3D organized hydrogel milieu[88]

Hybrid resins

Hybrid resins are emerging as promising materials for TPL as they offer benefits such as simple synthesis, modification, and processing. Besides, they exhibit high optical quality, chemical andelectrochemical inertness, and excellent mechanical and chemical stability. Ovsianikov et al. used silicon and zirconium alkoxides precursors to synthesise ultra-low shrinkage hybrid photosensitive resin. The ultra-low shrinkage was achieved by incorporating zirconium propoxide (ZPO) in the inorganic-organic sol-gel material (MAPTMS). This provides enough mechanical stability to the fabricated structures. The addition of ZPO contributed to enhanced photosensitivity of the resin.[93] Another experiment was reported by Franziska et al. in which a selectively functionalized scaffold for controlled 3D cell culture was fabricated by polymerizing PEGDA and OrmoComp, an inorganic-organic hybrid polymer, sequentially, by using direct-laser writing. As opposed to a mechanically unstable scaffold fabricated with surface-modified PEG, a mechanically stable and rigid protein-repellent scaffold was fabricated by using PEGDA doped with 4.8% polyacrylate cross-linking agent PETA as the photoresist. To functionalize this protein-repellent scaffold selectively, another protein-adsorbing photoresist was drop-cast onto it and sequentially photopolymerized. This resulted in the fabrication of selective protein-binding functionalized sites in a mechanically stable, protein-repellent matrix of PEGDA.[94] This approach was also used for other material combinations such as silicon and titanium alkoxide.[95] In contrast to the conventional sol-gel process–in which hydrolysis-condensation reaction is utilized toward inorganic polymerization– an experiment has been reported by Kustra et al., in which two-photon excitation was used to control the condensation reaction. The inorganic polymerization was controlled by adding photoacids or photo-baseto a pre-hydrolyzed monomer. This opens up the possibility of directly fabricating hybrid and inorganic materials using TPP, and the designed micro-ceramics.[95] Recently, Marini et al., have demonstrated bio-inspired 3D structures (osteo prints) in barium titanate NPs (BTNPs) doped OrmoComp resin. BTNPs were doped to impart piezoelectricity to the scaffolds.[92] The mechanical simulation provided by ultrasound wave enhanced the osteogenic differentiation of human SaOS-2 cells cultured in the scaffolds mimicking the structure of trabeculae of spongybone. Such piezoelectric scaffolds allow and provide means of remote actuation, to control the cell differentiation processes. Yu et al., demonstrated a micro-pressure sensor, based on TiO_2/carbon composite microstructure. Of interest, the conductivity of the structure was tuned by varying the laser fluence.[74] Such patterning of nanocomposites offers an easy method of integrating TiO_2/carbon composites in several microdevices. During laser writing, graphitization of organic molecules with titanium oxide precursor occurs. A carbon network is generated within TiO_2 matrix, leading to an increase in conductivity. Vyatskikith et al. demonstrated the fabrication of metallic nanostructures with resolution as high as 150 nm, and high metal content using a combination of TPL and pyrolysis.[72] Initially, microstructures were fabricated in the metal-polymer composite resin and then the structures were pyrolyzed to volatilize the organic compounds leaving metallic structures. The mechanical strength of these structures demonstrated mechanical strength in the range of 2.1–7.3 MPa g^{-1} cm^3. Such work holds potential in the development of miniature and complex metallic parts of devices such as microelectrodes in micro batteries, microbots, etc. Fe_3O_4 NP doped hydrogels were

employed for the fabrication of reversible light-responsive microactuators with a rapid response (~0.33 s for close/open), furthermore, the response was also dependent on the irradiation intensity.[16] Of interest, owing to the presence of Fe_3O_4 particles, microstructures can be actuated using a magnetic field. The implementation of doped/composite resin for additive manufacturing of microstructures using TPL provides a means for development of remotely controlled micro/nanodevices.

Polymerizable ionic liquid

Two-photon polymerization has also been employed in the fabrication of high-resolution 3D microstructures on soft, responsive polymer-type gels by employing poly (ionic liquids). Tudor et al. demonstrated the use of polymerizable ionic liquid monomers (PILs), a non-volatile liquid with excellent solubility for several materials such as PIs and cross-linkers, for the fabrication of microstructures.[96] Such microstructures incorporate the properties of parent ionic liquid such as tunable viscosity, excellent thermal/chemical stability, and high-charge density as well as the properties of the polymer such as the ability to form films and self-standing structures. Tributylhexyl phosphonium polysulfopropyl acrylate, polypropylene glycol diacrylate and diethylamino-3-thenoylcoumarin have been used as the ionic-liquid monomer, cross-linker and PI, respectively. The hydration of these microstructures results in significant expansion, which is a completely reversible behavior and hence various advanced functions such as the triggered release of functional micro-nanoparticles in a fluidic system and programmed movement, can be incorporated.[96]

Doped resins

Though significant advancement in TPP fabrication was realized within the early years of its development, the intrinsic limitations of polymers constrained its exhaustive applications. For example, the lower refractive index of polymers limits their usefulness in optics. It is known that the mechanical properties of polymers can significantly degrade in organic solvents or when processed at elevated temperatures. Besides, the toxicity of certain resin components (semiconductor quantum dots, dyes, etc.), can restrict their usage in biological applications. To further extend the integrity of the fabricated structures, researchers focused on adding stimuli-responsive functionality by incorporating suitable chemical, biological or optical species into the fabricated structures. This has been achieved by proper functionalization of the resin, which can be accomplished by several approaches as discussed below. The most conventional strategy of functionalization of fabricated microstructures involves dispersion of active material into resin for TPL. For example, fluorescent structures can be fabricated by incorporating suitable fluorophores (e.g., organic dyes, quantum dots, or luminescent nanoparticles) in the polymer matrix. *Correa* et al. fabricated microstructures containing rhodamine 610 dye in a resin consisting of a mixture of two triacrylate resins, tris(2-hydroxyethyl) isocyanurate triacrylate and ethoxylated (6) trimethylolpropane triacrylate. The emission characteristic of fluorophore indicated that the optical properties of the dye are retained in the microstructure, which is desirable for applications in photonic devices.[97] They also demonstrated the excitation of selected, individual microstructures by using micromanipulators and silica wires. This was the first step toward integration of a doped two-photon polymerized structure which opened the possibility of fabrication of micro-optical elements for photonic devices. Mendonca et al., demonstrated the fabrication of birefringent microstructures in the same resin, a mixture of triacrylate resins, tris(2-hydroxyethyl) isocyanurate triacrylate and ethoxylated (6) trimethylolpropane triacrylate. An azoaromatic dye - disperse red 13 (DR13), which is known to exhibit photo-induced birefringence, was doped in the photoresin.[98] In another experiment TPL was utilized to fabricate photonic defect structures in cholesteric liquid crystals (ChLCs) doped with a dye 4-(dicyanomethylene)-2methyl-6-(4-dimethylaminostryl)-4H-pyran (DCM).[99]

To fabricate 3D light-emitting nanostructures with emissions of different color light i.e., red (R), green (G), and blue (B), Peng et al. incorporated CdSe/ZnS/CdS based quantum dots in PETA.[91] The 3D microstructures showed 3D resolutions as small as 75 nm. The TPP of photoluminescent TPPRs can be used in the realization of nano emitters with fine control of spatial positioning of emission color. The second approach for functionalization involved doping of resin with the precursor of active materials that assist in two-photon polymerization. In some instances, *in situ* synthesis of active materials in the structure during photopolymerization is also possible. As an illustration, nanostructures containing gold nanoparticles (NPs), silver NPs and fluorescent NPs were fabricated by using this technique.[25,26,52,66,100–104] Another approach for functionalization of the polymerized structure involves covering it with a layer of active material. For instance, fabrication of metal-coated woodpile photonic crystal, operating in the near IR and optical regions, has been demonstrated by utilizing electroless plating metallization technique.[105,106] Carbon-based nanomaterials such as single-walled carbon nanotubes (SWCNTs) in polymers can enhance mechanical, thermal and electrical properties. Kawata et al. reported the fabrication of three-dimensional (3D)

Table 4. List of popular positive photo-resist monomers and photoinitiator, processing parameters and functionality of nano/microstructures fabricated using TPP

Resin	Photoinitiator	P (mW)	Speed (μm/s)	Resolution (nm)	Proposed Functionality	Reference
Novolak (AR-P3120)	DNQ	10–20	20	450	Fabrication over slanted platform	[109]
Novolac (AZ-4562)	DNQ	3.5	40	250	Microfluidic device	[110]
Novolak	DNQ	1–15	5–50	–	–	[111]
THPMA and MAA	bis[(diarylamino) styryl]benzene	0.4	–	–	3D microchannnel structures	[108]
AZ P4620 with NOVOLAC	DNQ	1.07 mW	10	95 nm	IC structures and nanodevices	[112]
AZ P4620 with NOVOLAC	DNQ	0.330 mW	–	85 nm	IC structures and nanodevices	[112]

*Laser writing power, **scan speed, DNQ: Diazonaphthoquinone, THPMA-3-Tetrahydrofurfuryloxy-2-hydroxypropyl methacrylate, IC: Integrating circuit, 3D: Three dimensions, MAA: Methacrylic acid.

micro-nanostructures using SWCNT/polymer composite by using TPL. It was found that higher resolution could be obtained in the composites as compared to that of the resin without SWCNTs. This can be attributed to the radical quencher produced by SWCNTs in the photo-resin, which led to the termination of the chain reaction in the process of photopolymerization. Also, it was found that SWCNTs were uniaxially aligned in a nanowire fabricated using this composite. Such an alignment enhances the mechanical stability as well as the electrical conductivity of the structure.[67] Another experiment was performed by the same group in which the alignment of SWCNTs was studied in detail and analyzed. It was found that SWCNTs aligned in the direction of laser scanning and the alignment could also be favored by tailoring the polarization of the laser beam. The ability to control the alignment of SWCNTs in any arbitrary direction in 3D micro-nanostructures would lead to new applications such as actuators and metamaterials.[24] The available literature describes the improvement in mechanical and electrical properties of the resins incorporating CNTs.[107]

The TPPRs discussed above sections are negative tone, i.e. the exposed regions of the resin become insoluble in the developer. The structure obtained after development shows the exact architectures, as scanned by the laser. Positive tone TPPRs produce a complementary structure to the laser exposed region by rendering the exposed two-photon processed volume soluble to the developer. Positive tone TPPRs are desirable for the fabrication of 3D structures containing minor voids, such as in 2D micro-holes and 3D microfluidic channels. It is much simpler, faster, efficient, and technically feasible to excavate and fabricate such structures rather than building walls/platforms with voids/channels. In addition, by the use of positive tone materials, it is possible to avoid shrinkage during fabrication/post-exposure development. Few authors have demonstrated the fabrication of microstructures using positive tone TPPR. Zhou et al. have implemented two-photon activated PACs based on [(diarylamino)styryl] benzene core with covalently attached sulfonium moieties for fabrication of 3D micro-channels and structures in chemically modified positive tone resist THPMA-MMA.[108]

Various commercially available positive tone photoresists based on Novolac have been used for the fabrication of micro/nanodevices. Details of a few popular positive photoresists used in TPL, writing parameters, and resolution of the fabricated structures are provided in Table 4. Cao et al., demonstrated one-step patterning of trenches with resolution as good as 85 nm in AZP4620, laying grounds for further development in the fabrication of subwavelength structures and nanodevices using PT-TPPRs.[112] A resolution of 95 nm was achieved using single scan and 1.07 mW power, whereas multiple scans using lower power ($\sim 0.330\ mW$) enabled in achieving a resolution of 85 nm. However, the effect of higher radiation dose was not explored/studied. Tsutsumi et al. systematically studied the lithographic characteristics at high power (upto 15 mW) and speeds upto 50 μmps; and demonstrated rapid prototyping of inverted 3D woodpile and helical structures.[113] van der Velden et al. used AZ4562 for the fabrication of microfluidic devices with two channels crossing each other at different heights and separated by membrane.[110] This was a crucial step toward the development of organ-on-chip technology for biomedical research. Heiskanen et al. showed fabrication of metallic lines over large areas using a combination of lithography and lift-off.[109] In PT-TPPR AR-P 3120, they also demonstrated the fabrication of metallic wires on complex 3D

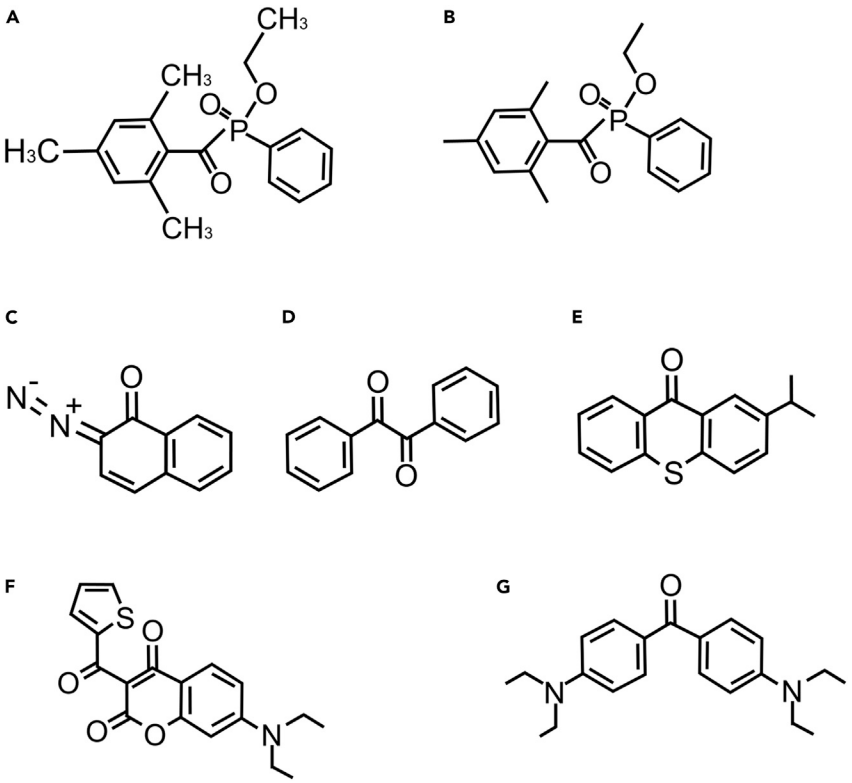

Figure 8. Chemical structures of the representative popular photoinitiators for TPL
(A). Ethyl-2,4,6- trimethylbenzoylphenylphosphinate,[27] (C). Irgacure 819,[91] (C). DNQ,[109] (D). Benzil,[16] (E). Isopropyl thioxanthone,[70] (F). 7-diethylamino-3-thenoylcoumarin[72] and (G). 4,4′- bis(diethylamino)benzophenone.[70].

structures using PT-TPPR and lift-off. With further developments in PT-TPPR-based fabrication, we envision an increase in the adoption of TPL in devices including monolithic integration of several nanocomponents to obtain organ-on-chip devices, microfluidic devices, and IC structures among others.

Photoinitiator (PI)

Two-photon photoinitiating system (TPPS) serves three main purposes: facilitation of two-photon up-conversion, initiation, and termination of crosslinking monomers/oligomers. Typically, a TPPS is composed of either PI, photoinhibitor, and PS or their combination. TPPS plays a crucial role in spatially localized TPA and transfer of the up-converted energy to the cross-linker/radical generator. The charge transfer between the PI and the monomer initiates the crosslinking process leading to the formation of polymerized voxels within the irradiated volume.

In recent years, a wide range of PI with good non-linear activity have been synthesized following the guidelines to design PIs with large TPA cross-sections.[114–119] The examples of few most popularly used PIs are ethyl-2,4,6- trimethylbenzoylphenylphosphinate,[27] Irgacure 819,[91] DNQ,[109] Benzil,[16] isopropyl thioxanthone,[70] 7-diethylamino-3-thenoylcoumarin[72] and 4,4′- bis(diethylamino)benzophenone.[70] Their chemical structures are shown in Figure 8.

Though these PIs have been used extensively in recent decades, there is a demand for a new generation of efficient materials that can serve as efficient PI. The most versatile approach to design a functional PI involves the incorporation of a suitable sensitizer with PI (e.g., fluorescent nanoparticles, dyes, semiconductor quantum dots) that can efficiently sensitize the PI. PI with a larger TPA cross-section does not ensure efficient execution of photoactivation/initiation of polymerization process. The radiative decay routes for the deactivation of excited states of PI must be minimized to accelerate the photo-polymerization process. Because of this reason, PIs with low fluorescent quantum yield are preferred, as non-radiative relaxation of excited states increases the probability of transfer of up-converted energy to the co-initiator, thereby enhancing the TPP sensitivity.[120] PI with a larger

TPA cross section and low fluorescent quantum yield (Φ_f) has been utilized to obtain TPP initiator with good TPP sensitivity. Usually, co-initiator molecules are anchored to the PI (PS) or ion pairing of initiators with absorbers to create intramolecular complexes. Such approaches yield TPPRs with fewer components and good TPP sensitivity which further ensures low polymerization threshold.[10,121–127] This results in reduced photoactivation volume and a low concentration of generated radicals that are required to initiatephoto-polymerization, thus eliminating the diffusion of the radicals and providing optimal resolutions and a large working window.[49] Furthermore, the resolution and quality of the structures can be improved by using optimal process parameters for fabricating the structures.

Applications

The micro/nanostructures fabricated using TPP 3D printing technique finds use in a wide range of applications such as in tissue engineering, micro-electromechanical systems, biomedical implants, microfluidics, micro/nano-photonics, and drug delivery.[29] An instance of tailoring microstructure properties according to desired application is in the biomedical and therapeutic area. Hydrophilic and bio-compatible structures of suitable functionality are required, but only a limited number of bio-compatible TPPRs are available. Thus the development of TPPRs for rapid prototyping of hierarchal structures with higher resolution and good throughput is in vogue. This section pertains to a discussion related to the applications of TPP-fabricated microstructures in various domains.

Micro-electromechanical devices

Recently, TPP fabrication method has been extensively explored for the fabrication of several micromechanical devices such as MEMS,[13] NEMS, microbots,[75] actuators,[16] micro- and nanofluidic devices.[14] As an instance, cylindrical and hexahedral-shaped microrobots were fabricated using epoxy-based SU-8 photo-resist. The fabricated microbots were used in targeted cell transportation applications.[128] Light-driven devices such as micro-springs[48] and cantilevers[15] have been fabricated in the early stages of TPP, and such stimuli-responsive systems have been rapidly developed since then.[13] Ip-S based photo-resist was used to fabricate 3D printed micro-scale bristle-bots (Figure 9A; weight 5 mg; dimensions 2 mm × 1.87 mm × 0.8 mm) that can carry on-board piezoelectric actuators.[75] Recently, Lander et al. designed micro-electro-mechanical systems (MEMS)-based miniaturized tensile testers that could measure the stress-strain response of the individual polymer nanowires as shown in Figures 9B and 9C. They fabricated the nanowires on the MEMS device to evaluate the mechanical properties of the nanowires. They found that at higher processing speed the Young's modulus and toughness of the structures reduced, because of low degree of polymer conversion. Xia et al. demonstrated smart micro/nanomachines by fabricating magnetically driven microturbine/micro-springs. They incorporated ferromagnetic particles as dopants in acrylate resin (PETA) that imparted magnetic attributes to the resin and the fabricated structures. The magnetic activity was tested by driving the micromachines under an external magnetic field.[68] Micrographs of the microturbine and the remote control of the microturbines can be seen in Figures 9D–9F. Zheng et al. have used photothermal poly(N-isopropylacrylamide) (PNIPAM)/nano-Fe_3O_4 hydrogels to fabricate a light-driven microactuator (size ~26 μm) that exhibits a fast light-response time.[16] The ON/OFF state of the microactuators is shown in Figures 9G and 9H. The displacement of the arms of the actuators was dependent on the intensity of the stimulating radiation, which can be seen in Figure 9I.

Vanderpoorten et al. demonstrated the integration of microfluidic and nanofluidic devices by fabricating two microchannels interconnected via nanochannel junctions in SU-8. They combined UV lithography and TPL for fabrication of these structures. The microchannels were fabricated using UV lithography and the nanochannels were fabricated by two-photon exposure. The SEM images of the fabricated structures are shown in image Figures 9J–9L.

Photonic and optoelectronic devices

In recent years, TPL manufacturing techniques have been developed to design optical waveguides,[11] photonic crystals,[64] SERS probes,[12] microlenses,[9] fluorescent structures[129] and plasmonic microstructures.[25,26] Shukla et al. demonstrated the generation of plasmonic nanostructures in gold-doped epoxy resin. These nanostructures exhibited structural chirality, as shown in the transmission microscope images in Figure 10A. The chirality of the structures was explored to rotate the field polarization. Theoretical analysis of the dependence of field rotation versus wavelength for a single element is shown in Figure 10B. Shukla et al. also demonstrated that the metal-polymer composite nanofibers generated via simultaneous photopolymerization and photoreduction were electrically conductive.[25] The nanofibers fabricated over gold electrodes are shown in Figure 10C, and the

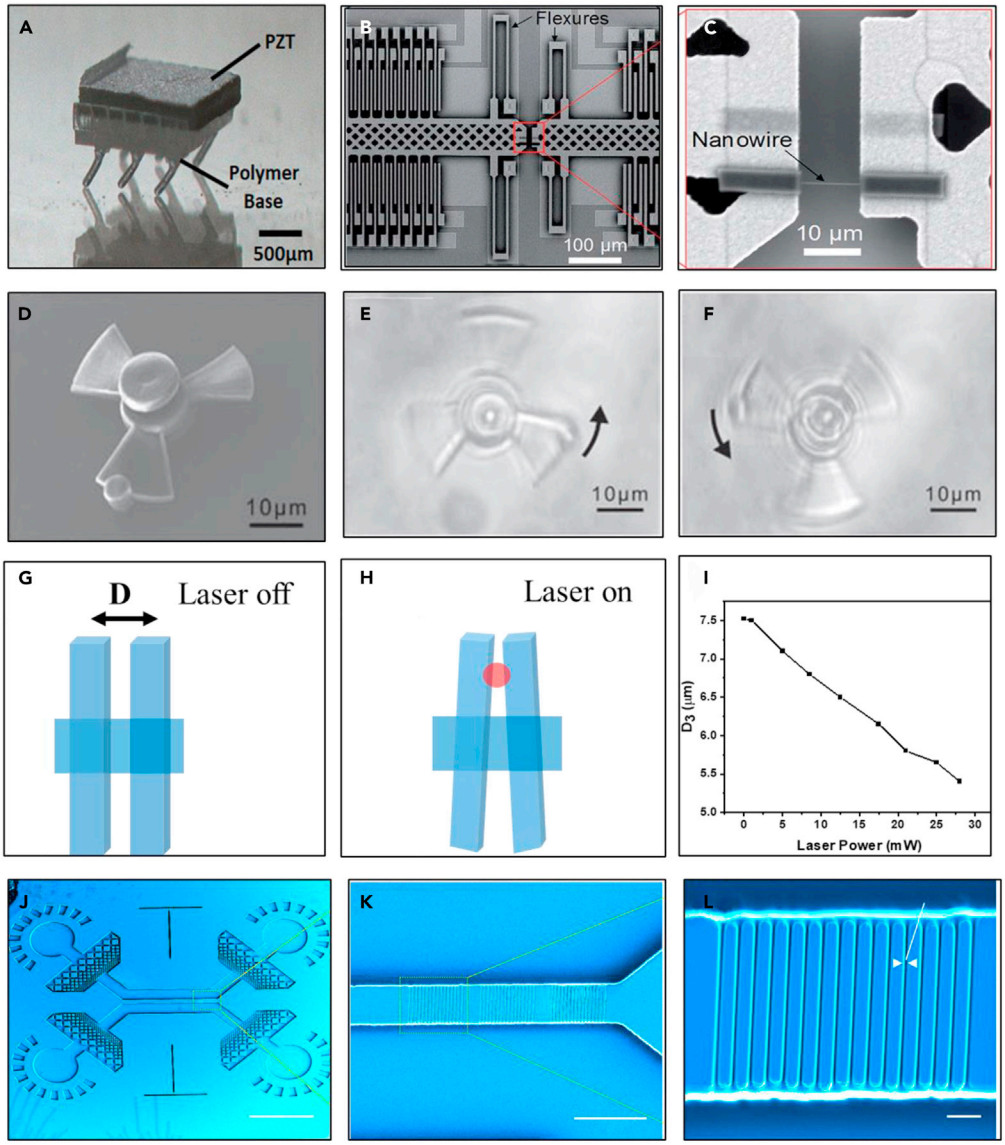

Figure 9. Various MEMS devices fabricated via TPL

(A). Micrograph of the 5 mg micro-bristle-bot,[75] (B and C). Micro-electro-mechanical systems (MEMS) based miniaturized tensile tester,[13] (D). SEM images of the microturbine,[68] (E and F).Optical microscopy images of the microturbine in a circumgyration cycle, (G and H) Model demonstrating light-driven hydrogel microactuator in absence and presence of laser beam, (I) Deflection versus average laser power in water for a hydrogel microcantilever (J–L). SEM images of nanofluidic PDMS imprint fabricated by the combination of UV mask lithography and 2-photon writing, (K) Three nanofluidic areas with nanochannels of 75-micron lengths joining the two microchannels, and (L) Higher magnification shows 420 nm wide nanochannels imprinted in PDMS.[14] Reprinted (adapted) with permissions from IOP Publishing Group, ref.[75], The Royal Society of Chemistry, ref. [13], Nature Publishing Group, ref. [14], and WILEY-VCH Verlag GmbH & Co., ref.[68].

plot of electric current versus applied voltage is shown in Figure 10D; the actual dimensions of the gold probes used for four-probe measurements are shown in the inset of Figure 10D. Jaiswal et al. used gold-acrylate composite to generate plasmonic mesh structures over a few mm.[130] These structures exhibited spectrally pure reflection as shown in the reflection image of the structure in Figure 10E. The theoretical calculations revealed a photonic bandgap as shown in Figure 10F. Nguyen et al. used an oligomer bisphenol– a diglycidyl ether-based resin to fabricate free-form waveguides. The fabricated waveguide exhibited a high index contrast of 0.013 between core and cladding with a transmission loss at 850 nm.[71] Furthermore, Fresnel micro-lens of 17 μm

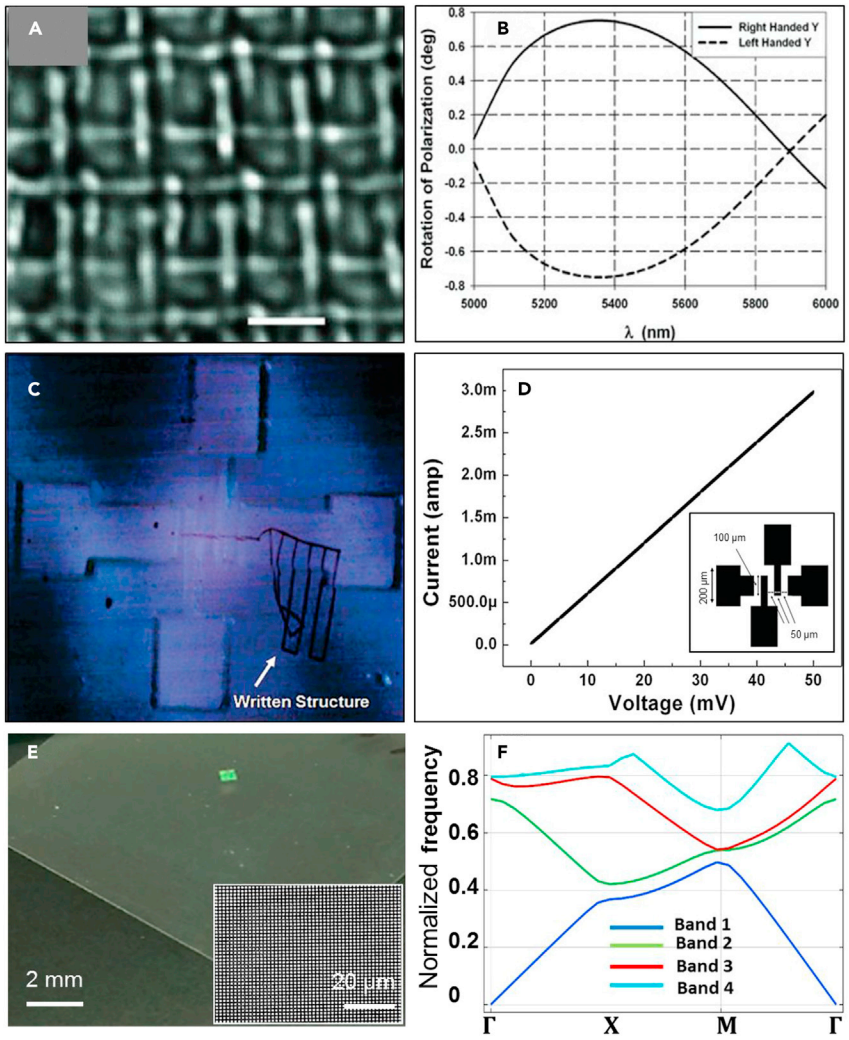

Figure 10. Metal-polymer composite nanostructures

(A) Optical microscope image of the chiral structures; scale bar = 4 µm, (B) Simulation of chiral structures showing field polarization rotation concerning wavelength in the transmitted field,[26] (C) Four probe measurements of epoxy-gold nanofiber, (D) Electrical characterization of current versus applied voltage, inset shows dimensions of four-point probe measurement system,[25] (E) Image of a large area 2D plasmonic mesh structure with a periodicity of 1.5 µm, fabricated in acrylate gold composite resin, showing the reflection of spectrally pure color under white light illumination; inset shows an optical microscope image of the structure and (F) Theoretical analysis of photonic band structure for the fabricated plasmonic structure; Γ, X and M are the high-symmetry points across the irreducible Brillouin zone.[135]Reprinted (adapted) with permissions from WILEY-VCH Verlag GmbH & Co., ref.[26], American Chemical Society, ref.[25], and Elsevier ref.,[130].

diameter was fabricated using an SCR500 photo-resist.[9] Tsutsumi et al. fabricated a micro-lens using the SU-8 photoresist. The focusing capability of the fabricated micro-lens was confirmed using the two-photon absorption fluorescence of an isopropyl thioxanthone (ITX) ethanol solution excited by a femtosecond Ti: Sapphire laser operating at 800 nm.[111] Ortiz-Huerta et al. developed a Fabry–Perot cavity using a combination of TPL and thermal evaporator deposition techniques. They built a polymer 'roof' of 15 µm x 15 µm with 4 polymer pillars to hold it at a determined height and a 20 nm thick silver layer was coated using a thermal evaporative deposition. The FIB image of the hybrid resonator is shown in Figure 11A. The fabricated cavity demonstrated resonant fluorescence emission. Malinauskas et al. fabricated micro spherical lenses with different radii of curvature on commercially available and widely used zirconium–silicon-based hybrid sol-gel photopolymer (Ormosil, SZ2080).[10] The fabricated microlenses were used to image macroscopic objects and it was found that the incorporation of the microlenses drastically enhanced the quality of the images. Kim et al. fabricated a fiber optic surface-enhanced Raman spectroscopy (SERS) probe (SERS-on-a-tip: SOT), with a diffraction grating-based surface

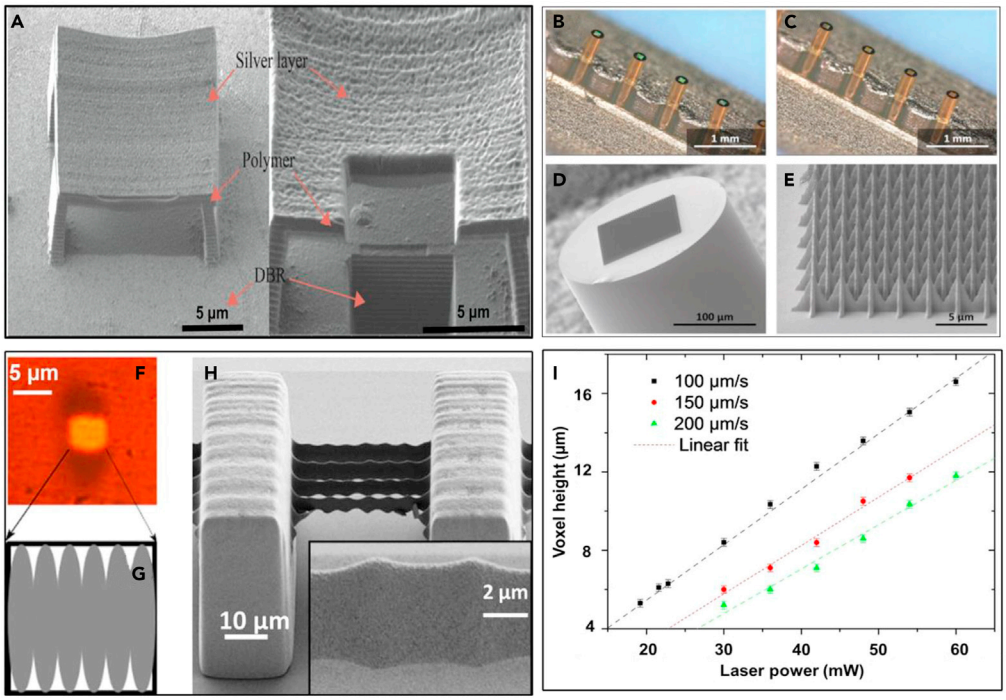

Figure 11. Nanopatterned active nanostructure

(A). FIB image of a hybrid Fabry-Pérot microcavity and cross-section of hybridmicrocavity showing a thickness of ~800 nm for the polymer/silver layer,[131] (B–E). Optical microphotographs and SEM images of SOTs.[12](F–H) End-facet image of a waveguide, multiple sweeping and side-view SEM micrograph of single lines after developing the unexposed resist,[71] (I). relation between input laser intensity and voxel height in direct laser writing at different writing speeds,[71] "Reprinted (adapted) with permissions from ref. 12, WILEY-VCH Verlag GmbH & Co., and ref. 71, ref. 131, Optica Publishing Group.

plasmon-polariton excitation mechanism.[12] TPL and subsequent metallization were used for the fabrication of these SERS probes. Optical images of SOTs with hexagonally arranged single-voxel array (HSVA) and cross spike array (CSA) are shown in Figure 11(b) and Figure 11(c), respectively. The SEM image of SOT tip and the zoomed view of CSA is shown in Figure 11(d) and Figure 11(e) respectively. The SOT was used for sensing low concentrations of rhodamine 6G dye. The detection limit was found to be in the range of 10^{-7} M and enhancement factors of up to 1300 were demonstrated.

Waveguides can be fabricated using TPL method followed by subsequent diffusion of monomer in the unexposed region (Nguyen et al.). The TPL resulted in the formation of a waveguide whereas the clad layer was formed because of monomer diffusion. The fabricated waveguide exhibited a high index-contrast of 0.013 between core and cladding with a transmission loss at 850 nm (transmission loss of ~0.37 dB/cm). The optical image of the end facets of the waveguide and the zoomed-in view in SEM micrographs are shown in Figures 11F–11H and the dependence of voxel size on average laser power is shown in Figure 11I. Houbertz et al. fabricated optical waveguides on inorganic-organic hybrid resin Ormocer.[11] Data transfer rates as high as 7 Gbit/s at a bit error ratio of about 10^{-9} were achieved for the fabricated waveguides. TPL has played a vital role in the development of active and passive components for optical and photonic applications and with the emergence of new TPPRs, further innovations are envisioned.

Bio-engineering devices

TPP-based structures offer a wide range of biomedical applications such as transdermal drug delivery, cell viability studies,[73] tissue engineering,[7] and bio-actuator devices.[16] In this direction, bio-degradable polymer, hydrogel, and a few hybrid materials were extensively explored.

The hydrogel-based photo-resists are suitable to fabricate 3D network of hydrophilic polymers. Their fascinating biochemical properties such as the presence of various functional groups and biocompatibility make them suitable for utilization in therapeutics, drug-delivery, and tissue engineering.

Polyethylene glycol (PEG) modified hydrogels have been explored for decades because of their unique properties such as ease of adding different functionalities, the low adsorption of protein and minimal inflammatory profile.[29] Zheng et al. demonstrated that PEG-based hydrogel can also be used for manufacturing bio-actuator devices which can be controlled by light. This was achieved by incorporating photothermal surface-modified Fe_3O_4 nanoparticles in the photoresist. The fabrication of 26 μm long microactuator was achieved and the light response time was approximately 0.033s. It was also found that the actuation response could be controlled with good repeatability.[16]

Ovsianikov et al. (2007) used polymer-ceramic hybrid material to fabricate hollow microneedles having a length of 800 μm and a base diameter of 150–300 μm for transdermal drug delivery applications.[6] Guo et al. demonstrated microstructures simulating the morphology of red blood cells at different angular tilts in PEGDA.[86] By varying TPL parameters, they were able to obtain structures with varying mechanical properties (Young's modulus varying in the range 3.50–6.52 MPa). Better control over mechanical strength is useful in designing cell scaffolds for cartilage repair.

Frederik et al. prepared scaffolds using biodegradable triblock copolymer poly(ε-caprolactone-co-trimethylenecarbonate)-b-poly(ethylene glycol)-b-poly(ε-caprolactoneco-trimethylenecarbonate). Cytotoxicity studies revealed that proliferation of cell was not affected by photopolymerization of the materials and could be employed in tissue-engineering.[7] Gittard et al. demonstrated the creation of polyethylene glycol-gentamicin sulfate microneedles by using two-photon polymerization micromoulding technique.[132] The fabricated structures, having reduced risk of infection, could be used in transdermal drug-delivery systems. The incorporation of gentamicin sulfate in the photoresist imparted antimicrobial properties to the fabricated structures.[54]

Franziska et al. designed a selectively functionalized scaffold using an inorganic-organic-based hybrid TPPR composed of PEGDA and OrmoComp for controlled 3D cell culture. It is to be noted that PEGDA-based TPPR (doped with 4.8% polyacrylate cross-linking agent PETA provided better mechanical stability to rigid protein repellent scaffold as opposed to surface modified PEG scaffold.

An implantable micro-caged device using an IP-Dip photoresist for controlled delivery of therapeutic agents at local sites has been explored. The drugs were encapsulated into needle-sized porous devices and delivered in a controlled manner to the targeted tissues.[79] Berwind et al. designed hydrophilic/hydrophobic biocompatible surfaces, using an IP-Dip photoresist. Recently, Versace et al. demonstrated functional microcages fabricated in acrylate based monomer pentaerythritol triacrylate (PETIA).[5] The structures exhibited bactericidal effects, with 95% bacteria mortality Figures 12A and 12B). Huang et al. implemented TPL for spatially confined DNA patterning of the microparticle surfaces. Spatially controlled irradiation of two-photon sensitive functional DNAs immobilized on the microparticles allowed cleaving/activation of the DNAs, leading to the generation of site-specific functionalization microparticles,[8] Figures 12C and 12D. To study the growth of cells in geometrically constrained environments, Larramendy et al. demonstrated scaffolds with microcontainers stacked over each other.[85] PC12 cells were successfully grown inside the micro scaffold. Such scaffolds can be used for differential culturing of cells at different layers and for studying the interaction between different cell types. With further functionalization, stimulus-responsive scaffolds can be designed and used for development of organ-on-chip device by incorporating 3D scaffolds with other microfluidic devices Figures 12E and 12F. A hydrogel containing an acetylacetone group was used as the photoactive system which was prepared by polymerization of acryloylacetone, acrylamide and N,N′-Methylene-bis-acrylamide. This demonstration of irreversible actuation of a cantilever deflection opened up the possibility of fabrication of movable 3D micromachine components and microfluidic systems which can be controlled optically.[15] However, conventional stimuli-responsive hydrogels respond slowly to the stimuli which results in hysteresis associated with on and off states. For smart materials, the response to stimuli should be fast and also reversible. Xiong et al. achieved this by using a novel asymmetric 3D multiphoton polymerization microfabrication technique (3D MPP).[16] In this technique, different parts of the fabricated microstructure possessed different polymerization degrees and hence this led to variable response sensitivity to water and aqueous salt solution. This facilitated controlled swelling, deformation, and bending behavior of the hydrogel. The photopolymerisable hydrogel precursor was prepared by dissolving monomer acrylamide and co-monomer AMPS along with cross-linker methylene-bis-acrylamide, PI benzil and photosensitizer 2-benyl-2-(dimethylamino)-4′-morpholinobutyrophenone in a hydrophilic solvent consisting of a mixture of methanol, DMSO and glycerol.

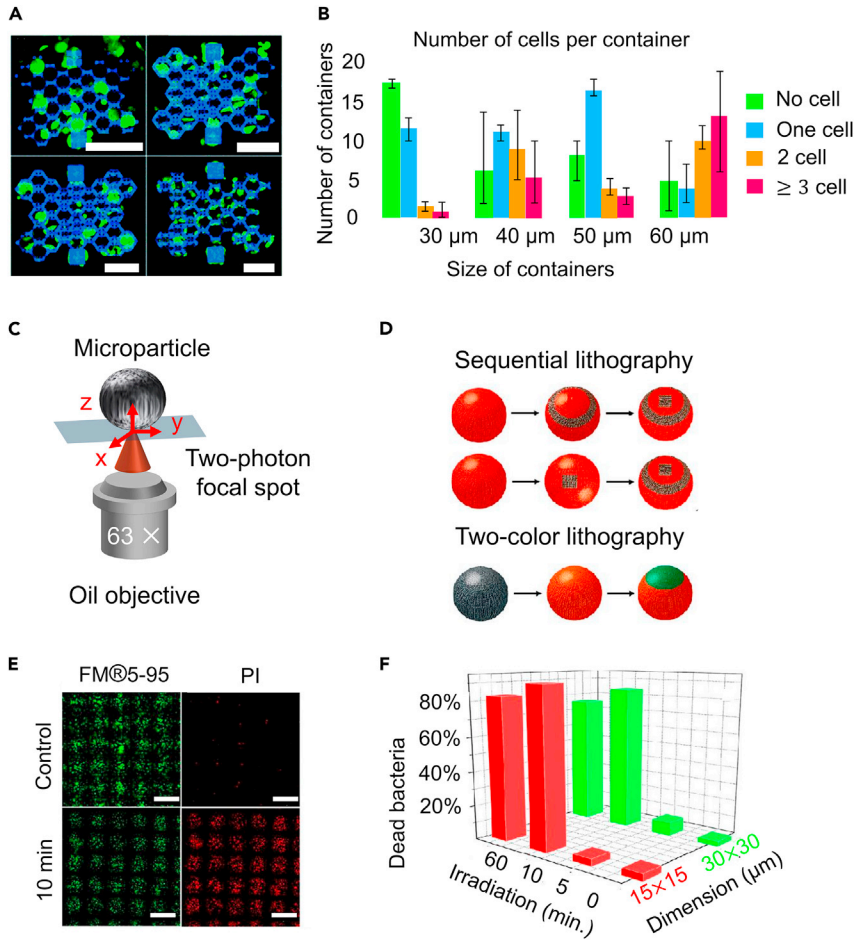

Figure 12. Two-photon lithography in bioengineering applications

(A) Confocal micrographs of the structure (blue fluorescence) with cultured cells (green fluorescence) after 2 days of culture on structures with different container dimensions. Container diameters: 30 μm, 40 μm, 50 μm, and 60 μm, (B) Bar graph of the number of cells per container, for (green) no cell, (blue) one cell, (orange) two cells, and (red) equal or greater than three cells, for a maximum of 32 containers, for container diameters of 30 μm, 40 μm, 50 μm, and 60 μm. Error bars indicate the maximum and minimum for each configuration,[85] (C) Schematic illustration of lithography (E) of DNA coated single microparticle surface, and (D) Sequential and two-colour writing on a single particle. DNA-coated single microparticle surfaces. Schematic cartoons showing the shape- and size-controlled (1, 2) and the sequential (3) and 2-colour (4) lithographic patterning of the particles. (E) Fluorescence microscopy images of bacteria trapped in microcages[5] and (F) The antibacterial activity of the microcages with respect to the cage dimensions and irradiation time.[5] scale bars in (a) and (e) are 100 μm and 15 μm, respectively. Reprinted (adapted) with permissions from ref. [85], The Royal Society of Chemistry, ref.[5], American Chemical Society, ref.[8].

A microcantilever was fabricated in this hydrogel by using asymmetric 3D MPP technique. It was found that controlled bending could be achieved in a water medium and the bending direction could be reversed by using an aqueous solution of NaCl. Moreover, the original condition could be achieved by changing the medium from NaCl to water. The bending behavior was also influenced by the length of cantilever. The ion-response time of the cantilever was 0.133s, which was very short as compared to that of macroscale hydrogel. 3D microstructures of stimuli-responsive hydrogel can be used in fabrication of biomedical microdevices, microactuators and micromanipulators.[133] Because water content in hydrogels is similar to that of soft tissues and they can mimic the chemical, biological, and mechanical properties of native tissues. Therefore, hydrogels are widely employed in scaffold fabrication for tissue engineering and drug-delivery.

The recent innovation in organic and genetically encoded fluorescent dyes and the technical development in microscopy and photonics have brought significant advancement in the field of biological imaging. The

dye-doped resins were used to fabricate fluorescent structures capable of monitoring several parameters such as the growth of cells and their migration behavior, DNA, RNA, sub-cellular species, proteins, and so forth. Costantino et al. demonstrated that polymerized structures incorporating luminescent dye can be used in adherent cell matrices and serve as fluorescent markers.[129] They fabricated luminescent arrays of micrometre dimensions on the glass coverslip using TPL and demonstrated that the fluorescence and topography of these biomarkers can be utilized in calibrating units composed of fluorescence probe detection and scanning probe microscopy for near field scanning probe microscopy. The utilization of micro-lithograph substrates in micro-contact printing (μCP) can provide a new approach to achieve protein patterns. The doped dye was used as a label to stain solidified structures which have provided an effective two-photon fluorescence technique for internal micro-diagnosis of polymerized 3D microstructures. The application of TPL to tailor the micro-contact printing structures with predetermined fluorescence and topography has not been explored extensively until date for biophysical applications.

CONCLUSION AND OUTLOOK

In this review, we have presented a comprehensive overview of recent advancements in TPL-based 3D printing of micro/nanoscale devices. Special attention has been given to discuss design strategies for the formulations of resins and PI to achieve improved TPP sensitivity. Furthermore, the strategies to control TPL process parameters to obtain optimal 3D patterning with the best achievable resolution have been discussed regarding their applications in micro/nanophotonics, MEMS, metamaterials and biomedical applications among others. We have discussed the role of incorporation of dopants (e.g., metal/carbon nanoparticles, dyes, semiconductor quantum dots, and biomolecules) into photo-resist PI, to impart additional functional characteristics to the fabricated micro/nanostructures. With present technology and available TPPRs, the true potential of TPL fabrication is constrained because of low writing speed, small processing volumes and the complexity of the materials system arising because of multiple component formulations of the PI and PR. Though the synthesis protocols for designing PI and PR materials are well established, their complex synthesis procedure forms a bottleneck.

The synergistic advancements in material science, optics and laser technology are pivotal for further progress of TPL-based additive manufacturing and their potential practical applications. Development of novel functional materials with good TPP sensitivity and minimal material components are expected to drive TPL toward fabrication of monolithically integrated devices such as lab-on-a-chip sensors and actuators. The incorporation of stimuli-responsive functional groups to the resin can be exploited for fabrication of externally controlled/driven micro/nanomachines applicable in biomedical and therapeutic applications, microfluidic devices, microreactors. Further research and development into materials can be directed toward the development of smart materials programmed to deform-reconfigure in response to the changes in the local environment, leading to the application of TPL in next-generation, self-driven micromachines. On the other hand, advancements in optics and laser technology are envisioned to offer new classes of lasers with higher average laser powers and, engineered optical components can be exploited to attain scalable fabrication with improved throughput. For, instance the parallel printing TPL process is still limited to a few spots processed at once because of the small focal volume of the objective lens. However, an array of miniature, planar, focusing elements in combination with collimated laser beams can be incorporated to counter these issues. This will assist in increasing the throughput of the TPL printer. With the encouraging results, contributions from enthusiastic researchers and technological advancements we can envisage a paradigm shift and accelerated development in additive manufacturing of 3D micro/nanoscale structures, leading to advancement in fundamental sciences, engineering and medical science in near future.

ACKNOWLEDGMENTS

The authors would like to acknowledge financial support from the Department of Science and Technology, Ministry of Science and Technology, through grant no. DST/INT/AUS/P-82/2022(G), grant no. DST/TM/WTI/WIC/2K17/100(C), Science and Engineering Research Board (SERB) grant no. EMR/2017/005144 and Department of Science and Technology, Solar Energy Research Initiative (SERI), Government of India, with a grant via sanction order no. DST/TM/SERI/2k10/12/(G) for this work.

AUTHOR CONTRIBUTIONS

A.J. and C.K.R: Writing – original draft, Formal analysis, Validation, Investigation, Project administration; S.R. and G.P.S.: Writing – original draft, Data curation, Formal analysis. S.S.: Writing – review and editing,

Supervision, Funding acquisition, Project administration. S.S.: Writing – review and editing, Supervision, Conceptualization, Funding acquisition, Project administration.

DECLARATION OF INTERESTS

The authors declare that they have no known competing financial interests or personal relationships that could have appeared to influence the work reported in this paper.

REFERENCES

1. Teh, W.H., Dürig, U., Drechsler, U., Smith, C.G., and Güntherodt, H.J. (2005). Effect of low numerical-aperture femtosecond two-photon absorption on (SU-8) resist for ultrahigh-aspect-ratio microstereolithography. J. Appl. Phys. *97*, 054907. https://doi.org/10.1063/1.1856214.

2. Lee, T.W., Mitrofanov, O., and Hsu, J.W.P. (2005). Pattern-transfer fidelity in soft lithography: the role of pattern density and aspect ratio. Adv. Funct. Mater. *15*, 1683–1688. https://doi.org/10.1002/adfm.200400295.

3. Verbitsky, L., Waiskopf, N., Magdassi, S., and Banin, U. (2019). A clear solution: semiconductor nanocrystals as photoinitiators in solvent free polymerization. Nanoscale *11*, 11209–11216. https://doi.org/10.1039/c9nr03086g.

4. Pawar, A.A., Halivni, S., Waiskopf, N., Ben-Shahar, Y., Soreni-Harari, M., Bergbreiter, S., Banin, U., and Magdassi, S. (2017). Rapid three-dimensional printing in water using semiconductor-metal hybrid nanoparticles as photoinitiators. Nano Lett. *17*, 4497–4501. https://doi.org/10.1021/acs.nanolett.7b01870.

5. Versace, D.L., Moran, G., Belqat, M., Spangenberg, A., Méallet-Renault, R., Abbad-Andaloussi, S., Brezová, V., and Malval, J.P. (2020). Highly virulent bactericidal effects of curcumin-based μ-cages fabricated by two-photon polymerization. ACS Appl. Mater. Interfaces *12*, 5050–5057. https://doi.org/10.1021/acsami.9b18693.

6. Ovsianikov, A., Chichkov, B., Mente, P., Monteiro-Riviere, N.A., Doraiswamy, A., and Narayan, R.J. (2007). Two photon polymerization of polymer-ceramic hybrid materials for transdermal drug delivery. Int. J. Appl. Ceram. Technol. *4*, 22–29. https://doi.org/10.1111/j.1744-7402.2007.02115.x.

7. Claeyssens, F., Hasan, E.A., Gaidukeviciute, A., Achilleos, D.S., Ranella, A., Reinhardt, C., Ovsianikov, A., Shizhou, X., Fotakis, C., Vamvakaki, M., et al. (2009). Three-dimensional biodegradable structures fabricated by two-photon polymerization. Langmuir *25*, 3219–3223. https://doi.org/10.1021/la803803m.

8. Huang, F., Zhang, J., Li, T., Duan, R., Xia, F., and Willner, I. (2019). Two-photon lithographic patterning of DNA-coated single-microparticle surfaces. Nano Lett. *19*, 618–625. https://doi.org/10.1021/acs.nanolett.8b04975.

9. Guo, R., Xiao, S., Zhai, X., Li, J., Xia, A., and Huang, W. (2006). Micro lens fabrication by means of femtosecond two photon photopolymerization. Opt Express *14*, 810–816. https://doi.org/10.1364/opex.14.000810.

10. Malinauskas, M., Gilbergs, H., Ukauskas, A., Purlys, V., Paipulas, D., and Gadonas, R. (2010). A femtosecond laser-induced two-photon photopolymerization technique for structuring microlenses. J. Opt. *12*, 035204. https://doi.org/10.1088/2040-8978/12/3/035204.

11. Houbertz, R., Satzinger, V., Schmid, V., Leeb, W., and Langer, G. (2008). Optoelectronic printed circuit board: 3D structures written by two-photon absorption. Org. 3D Photonics Mater. Devices II *7053*, 70530B. https://doi.org/10.1117/12.798817.

12. Kim, J.A., Wales, D.J., Thompson, A.J., and Yang, G. (2020). Fiber-optic sers probes fabricated using two-photon polymerization for rapid detection of bacteria. Adv. Opt. Mater. *8*, 1901934. https://doi.org/10.1002/adom.201901934.

13. Ladner, I.S., Cullinan, M.A., and Saha, S.K. (2019). Tensile properties of polymer nanowires fabricated: via two-photon lithography. RSC Adv. *9*, 28808–28813. https://doi.org/10.1039/c9ra02350j.

14. Vanderpoorten, O., Peter, Q., Challa, P.K., Keyser, U.F., Baumberg, J., Kaminski, C.F., and Knowles, T.P.J. (2019). Scalable integration of nano-and microfluidics with hybrid two-photon lithography. Microsyst. Nanoeng. *5*, 40. https://doi.org/10.1038/s41378-019-0080-3.

15. Watanabe, T., Akiyama, M., Totani, K., Kuebler, S.M., Stellacci, F., Wenseleers, W., Braun, K., Marder, S.R., and Perry, J.W. (2002). Photoresponsive hydrogel microstructure fabricated by two-photon initiated polymerization. Adv. Funct. Mater. *12*, 611–614. https://doi.org/10.1002/1616-3028(20020916)12:9<611::AID-ADFM611>3.0.CO;2-3.

16. Zheng, C., Jin, F., Zhao, Y., Zheng, M., Liu, J., Dong, X., Xiong, Z., Xia, Y., and Duan, X. (2020). Light-driven micron-scale 3D hydrogel actuator produced by two-photon polymerization microfabrication. Sensor. Actuator. B Chem. *304*, 127345. https://doi.org/10.1016/j.snb.2019.127345.

17. Joshi, M.P., Pudavar, H.E., Swiatkiewicz, J., Prasad, P.N., and Reianhardt, B.A. (1999). Three-dimensional optical circuitry using two-photon-assisted polymerization. Appl. Phys. Lett. *74*, 170–172. https://doi.org/10.1063/1.123283.

18. Serbin, J., Ovsianikov, A., and Chichkov, B. (2004). Fabrication of woodpile structures by two-photon polymerization and investigation of their optical properties. Opt Express *12*, 5221–5228. https://doi.org/10.1364/opex.12.005221.

19. Zhong, Y., and Wong, K.S. (2007). Fabrication of photonic crystal by two-photon single-beam laser holographic lithography. In Conference on Lasers and Electro-Optics, 2007, CLEO 2007. https://doi.org/10.1109/CLEO.2007.4453434.

20. Tayalia, P., Mendonca, C.R., Baldacchini, T., Mooney, D.J., and Mazur, E. (2008). 3D cell-migration studies using two-photon engineered polymer scaffolds. Adv. Mater. *20*, 4494–4498. https://doi.org/10.1002/adma.200801319.

21. Hsieh, T.M., Ng, C.W.B., Narayanan, K., Wan, A.C.A., and Ying, J.Y. (2010). Three-dimensional microstructured tissue scaffolds fabricated by two-photon laser scanning photolithography. Biomaterials *31*, 7648–7652. https://doi.org/10.1016/j.biomaterials.2010.06.029.

22. Farsari, M., and Chichkov, B.N. (2009). Materials processing: two-photon fabrication. Nat. Photonics *3*, 450–452. https://doi.org/10.1038/nphoton.2009.131.

23. Kunwar, P., Turquet, L., Hassinen, J., Ras, R.H.A., Toivonen, J., and Bautista, G. (2016). Holographic patterning of fluorescent microstructures comprising silver nanoclusters. Opt. Mater. Express *6*, 946. https://doi.org/10.1364/ome.6.000946.

24. Ushiba, S., Shoji, S., Masui, K., Kono, J., and Kawata, S. (2014). Direct laser writing of 3D architectures of aligned carbon nanotubes. Adv. Mater. *26*, 5653–5657. https://doi.org/10.1002/adma.201400783.

25. Shukla, S., Furlani, E.P., Vidal, X., Swihart, M.T., and Prasad, P.N. (2010). Two-photon lithography of sub-wavelength metallic structures in a polymer matrix. Adv. Mater. *22*, 3695–3699. https://doi.org/10.1002/adma.201000059.

26. Shukla, S., Vidal, X., Furlani, E.P., Swihart, M.T., Kim, K.T., Yoon, Y.K., Urbas, A., and Prasad, P.N. (2011). Subwavelength direct laser patterning of conductive gold nanostructures by simultaneous photopolymerization and photoreduction. ACS Nano *5*, 1947–1957. https://doi.org/10.1021/nn103015g.

27. Chaudhary, R.P., Ummethala, G., Jaiswal, A., Hawal, S., Saxena, S., and Shukla, S. (2016). One-step, subwavelength patterning of plasmonic gratings in metal-polymer composites. RSC Adv. *6*, 113457–113462. https://doi.org/10.1039/c6ra22604c.

28. Wloka, T., Gottschaldt, M., and Schubert, U.S. (2022). From light to structure: photo initiators for radical two-photon polymerization. Chemistry *28*, e202104191. https://doi.org/10.1002/chem.202104191.

29. Liao, C., Wuethrich, A., and Trau, M. (2020). A material odyssey for 3D nano/microstructures: two photon polymerization based nanolithography in bioapplications. Appl. Mater. Today *19*, 100635. https://doi.org/10.1016/j.apmt.2020.100635.

30. Carlotti, M., and Mattoli, V. (2019). Functional materials for two-photon polymerization in microfabrication. Small *15*, 1902687. https://doi.org/10.1002/smll.201902687.

31. Lay, C.L., Koh, C.S.L., Lee, Y.H., Phan-Quang, G.C., Sim, H.Y.F., Leong, S.X., Han, X., Phang, I.Y., and Ling, X.Y. (2020). Two-photon-assisted polymerization and reduction: emerging formulations and applications. ACS Appl. Mater. Interfaces *12*, 10061–10079. https://doi.org/10.1021/acsami.9b20911.

32. Lao, Z., Xia, N., Wang, S., Xu, T., Wu, X., and Zhang, L. (2021). Tethered and untethered 3d microactuators fabricated by two-photon polymerization: a review. Micromachines *12*, 465. https://doi.org/10.3390/mi12040465.

33. Wang, X., Wei, Z., Baysah, C.Z., Zheng, M., and Xing, J. (2019). Biomaterial-based microstructures fabricated by two-photon polymerization microfabrication technology. RSC Adv. *9*, 34472–34480. https://doi.org/10.1039/c9ra05645a.

34. Ciuciu, A.I., and Cywiński, P.J. (2014). Two-photon polymerization of hydrogels-versatile solutions to fabricate well-defined 3D structures. RSC Adv. *4*, 45504–45516. https://doi.org/10.1039/c4ra06892k.

35. Otuka, A.J.G., Tomazio, N.B., Paula, K.T., and Mendonça, C.R. (2021). Two-photon polymerization: functionalized microstructures, micro-resonators, and bio-scaffolds. Polymers *13*, 1994. https://doi.org/10.3390/polym13121994.

36. Huang, Z., Chi-Pong Tsui, G., Deng, Y., and Tang, C.Y. (2020). Two-photon polymerization nanolithography technology for fabrication of stimulus-responsive micro/nano-structures for biomedical applications. Nanotechnol. Rev. *9*, 1118–1136. https://doi.org/10.1515/ntrev-2020-0073.

37. Lemma, E.D., Spagnolo, B., De Vittorio, M., and Pisanello, F. (2019). Studying cell mechanobiology in 3D: the two-photon lithography approach. Trends Biotechnol. *37*, 358–372. https://doi.org/10.1016/j.tibtech.2018.09.008.

38. Harinarayana, V., and Shin, Y.C. (2021). Two-photon lithography for three-dimensional fabrication in micro/nanoscale regime: a comprehensive review. Opt Laser. Technol. *142*, 107180. https://doi.org/10.1016/j.optlastec.2021.107180.

39. Nguyen, A.K., and Narayan, R.J. (2017). Two-photon polymerization for biological applications. Mater. Today *20*, 314–322. https://doi.org/10.1016/j.mattod.2017.06.004.

40. Narayan, R.J., Doraiswamy, A., Chrisey, D.B., and Chichkov, B.N. (2010). Medical prototyping using two photon polymerization. Mater. Today *13*, 42–48. https://doi.org/10.1016/S1369-7021(10)70223-6.

41. Song, J., Michas, C., Chen, C.S., White, A.E., and Grinstaff, M.W. (2020). From simple to architecturally complex hydrogel scaffolds for cell and tissue engineering applications: opportunities presented by two-photon polymerization. Adv. Healthc. Mater. *9*, 1901217. https://doi.org/10.1002/adhm.201901217.

42. Lin, Y., and Xu, J. (2018). Microstructures fabricated by two-photon polymerization and their remote manipulation techniques: toward 3d printing of micromachines. Adv. Opt. Mater. *6*, 1701359. https://doi.org/10.1002/adom.201701359.

43. Torgersen, J., Qin, X.H., Li, Z., Ovsianikov, A., Liska, R., and Stampfl, J. (2013). Hydrogels for two-photon polymerization: a toolbox for mimicking the extracellular matrix. Adv. Funct. Mater. *23*, 4542–4554. https://doi.org/10.1002/adfm.201203880.

44. Selimis, A., Mironov, V., and Farsari, M. (2015). Direct laser writing: principles and materials for scaffold 3D printing. Microelectron. Eng. *132*, 83–89. https://doi.org/10.1016/j.mee.2014.10.001.

45. Zhou, X., Hou, Y., and Lin, J. (2015). A review on the processing accuracy of two-photon polymerization. AIP Adv. *5*, 030701. https://doi.org/10.1063/1.4916886.

46. Kiefer, P., Hahn, V., Nardi, M., Yang, L., Blasco, E., Barner-Kowollik, C., and Wegener, M. (2020). Sensitive photoresists for rapid multiphoton 3d laser micro- and nanoprinting. Adv. Opt. Mater. *8*, 2000895. https://doi.org/10.1002/adom.202000895.

47. Chaudhary, R.P., Jaiswal, A., Ummethala, G., Hawal, S.R., Saxena, S., and Shukla, S. (2017). Sub-wavelength lithography of complex 2D and 3D nanostructures without two-photon dyes. Addit. Manuf. *16*, 30–34. https://doi.org/10.1016/j.addma.2017.05.003.

48. Kawata, S., Sun, H.B., Tanaka, T., and Takada, K. (2001). Finer features for functional microdevices. Nature *412*, 697–698. https://doi.org/10.1038/35089130.

49. Ummethala, G., Jaiswal, A., Chaudhary, R.P., Hawal, S., Saxena, S., and Shukla, S. (2017). Localized polymerization using single photon photoinitiators in two-photon process for fabricating subwavelength structures. Polymer *117*, 364–369. https://doi.org/10.1016/j.polymer.2017.04.039.

50. Maruo, S., and Kawata, S. (1997). Two-photon-absorbed photopolymerization for three-dimensional microfabrication. Proc. IEEE Micro Electro Mech. Syst. *22*, 169–174. https://doi.org/10.1109/memsys.1997.581794.

51. Bhawalkar, J.D., He, G.S., and Prasad, P.N. (1996). Nonlinear multiphoton processes in organic and polymeric materials. Rep. Prog. Phys. *59*, 1041–1070. https://doi.org/10.1088/0034-4885/59/9/001.

52. Jaiswal, A., Rani, S., Singh, G.P., Hassan, M., Nasrin, A., Gomes, V.G., Saxena, S., and Shukla, S. (2021). Additive manufacturing of highly fluorescent organic 3D-metastructures at sub-wavelength resolution. Mater. Today Phys. *20*, 100434. https://doi.org/10.1016/j.mtphys.2021.100434.

53. Hahn, V., Kiefer, P., Frenzel, T., Qu, J., Blasco, E., Barner-Kowollik, C., and Wegener, M. (2020). Rapid assembly of small materials building blocks (voxels) into large functional 3D metamaterials. Adv. Funct. Mater. *30*, 1907795. https://doi.org/10.1002/adfm.201907795.

54. Matsuo, S., Juodkazis, S., and Misawa, H. (2005). Femtosecond laser microfabrication of periodic structures using a microlens array. Appl. Phys. A *80*, 683–685. https://doi.org/10.1007/s00339-004-3108-x.

55. Kato, J.I., Takeyasu, N., Adachi, Y., Sun, H.B., and Kawata, S. (2005). Multiple-spot parallel processing for laser micronanofabrication. Appl. Phys. Lett. *86*, 044102. https://doi.org/10.1063/1.1855404.

56. Frantz, C., Stewart, K.M., and Weaver, V.M. (2010). The extracellular matrix at a glance. J. Cell Sci. *123*, 4195–4200. https://doi.org/10.1242/jcs.023820.

57. Juodkazis, S., Mizeikis, V., Seet, K.K., Miwa, M., and Misawa, H. (2005). Two-photon lithography of nanorods in SU-8 photoresist. Nanotechnology *16*, 846–849. https://doi.org/10.1088/0957-4484/16/6/039.

58. Tan, D., Li, Y., Qi, F., Yang, H., Gong, Q., Dong, X., and Duan, X. (2007). Reduction in feature size of two-photon polymerization using SCR500. Appl. Phys. Lett. *90*, 071106–71114. https://doi.org/10.1063/1.2535504.

59. Park, S.H., Lee, S.H., Yang, D.Y., Kong, H.J., and Lee, K.S. (2005). Subregional slicing method to increase three-dimensional nanofabrication efficiency in two-photon polymerization. Appl. Phys. Lett. *87*, 154108–154113. https://doi.org/10.1063/1.2103393.

60. Jeon, S., Malyarchuk, V., Rogers, J.A., and Wiederrecht, G.P. (2006). Fabricating three-dimensional nanostructures using two photon lithography in a single exposure step. Opt Express *14*, 2300–2308. https://doi.org/10.1364/oe.14.002300.

61. Haske, W., Chen, V.W., Hales, J.M., Dong, W., Barlow, S., Marder, S.R., and Perry, J.W. (2007). 65 nm feature sizes using visible wavelength 3-D multiphoton lithography.

Opt Express *15*, 3426–3436. https://doi.org/10.1364/oe.15.003426.

62. Chu, W., Tan, Y., Wang, P., Xu, J., Li, W., Qi, J., and Cheng, Y. (2018). Centimeter-height 3D printing with femtosecond laser two-photon polymerization. Adv. Mater. Technol. *3*, 1700396. https://doi.org/10.1002/admt.201700396.

63. Saha, S.K., Wang, D., Nguyen, V.H., Chang, Y., Oakdale, J.S., and Chen, S.C. (2019). Scalable submicrometer additive manufacturing. Science *366*, 105–109. https://doi.org/10.1126/science.aax8760.

64. Ohlinger, K., Torres, F., Lin, Y., Lozano, K., Xu, D., and Chen, K.P. (2010). Photonic crystals with defect structures fabricated through a combination of holographic lithography and two-photon lithography. J. Appl. Phys. *108*, 073113–073115. https://doi.org/10.1063/1.3493119.

65. Fujishiro, Y., Furukawa, T., and Maruo, S. (2020). Simple autofocusing method by image processing using transmission images for large-scale two-photon lithography. Opt Express *28*, 12342–12351. https://doi.org/10.1364/oe.390486.

66. Sun, Z.B., Dong, X.Z., Chen, W.Q., Nakanishi, S., Duan, X.M., and Kawata, S. (2008). Multicolor polymer nanocomposites: in situ synthesis and fabrication of 3D microstructures. Adv. Mater. *20*, 914–919. https://doi.org/10.1002/adma.200702035.

67. Ushiba, S., Shoji, S., Masui, K., Kuray, P., Kono, J., and Kawata, S. (2013). 3D microfabrication of single-wall carbon nanotube/polymer composites by two-photon polymerization lithography. Carbon *59*, 283–288. https://doi.org/10.1016/j.carbon.2013.03.020.

68. Xia, H., Wang, J., Tian, Y., Chen, Q.D., Du, X.B., Zhang, Y.L., He, Y., and Sun, H.B. (2010). Ferrofluids for fabrication of remotely controllable micro-nanomachines by two-photon polymerization. Adv. Mater. *22*, 3204–3207. https://doi.org/10.1002/adma.201000542.

69. Brodeur, A., and Chin, S.L. (1999). Ultrafast white-light continuum generation and self-focusing in transparent condensed media. J. Opt. Soc. Am. B *16*, 637. https://doi.org/10.1364/josab.16.000637.

70. Arnoux, C., Konishi, T., Van Elslande, E., Poutougnigni, E.A., Mulatier, J.C., Khrouz, L., Bucher, C., Dumont, E., Kamada, K., Andraud, C., et al. (2020). Polymerization photoinitiators with near-resonance enhanced two-photon absorption cross-section: toward high-resolution photoresist with improved sensitivity. Macromolecules *53*, 9264–9278. https://doi.org/10.1021/acs.macromol.0c01518.

71. Duc Nguyen, H.H., Hollenbach, U., Ostrzinski, U., Pfeiffer, K., Hengsbach, S., and Mohr, J. (2016). Freeform three-dimensional embedded polymer waveguides enabled by external-diffusion assisted two-photon lithography. Appl. Opt. *55*, 1906–1912. https://doi.org/10.1364/ao.55.001906.

72. Vyatskikh, A., Ng, R.C., Edwards, B., Briggs, R.M., and Greer, J.R. (2020). Additive manufacturing of high-refractive-index, nanoarchitected titanium dioxide for 3d dielectric photonic crystals. Nano Lett. *20*, 3513–3520. https://doi.org/10.1021/acs.nanolett.0c00454.

73. Brigo, L., Urciuolo, A., Giulitti, S., Della Giustina, G., Tromayer, M., Liska, R., Elvassore, N., and Brusatin, G. (2017). 3D high-resolution two-photon crosslinked hydrogel structures for biological studies. Acta Biomater. *55*, 373–384. https://doi.org/10.1016/j.actbio.2017.03.036.

74. Yu, S.Y., Schrodj, G., Mougin, K., Dentzer, J., Malval, J.P., Zan, H.W., Soppera, O., and Spangenberg, A. (2018). Direct laser writing of crystallized TiO2 and TiO2/carbon microstructures with tunable conductive properties. Adv. Mater. *30*, e1805093–e1805098. https://doi.org/10.1002/adma.201805093.

75. Kim, D., Hao, Z., Ueda, J., and Ansari, A. (2019). A 5 mg micro-bristle-bot fabricated by two-photon lithography. J. Micromech. Microeng. *29*, 105006. https://doi.org/10.1088/1361-6439/ab309b.

76. LaFratta, C.N., Baldacchini, T., Farrer, R.A., Fourkas, J.T., Teich, M.C., Saleh, B.E.A., and Naughton, M.J. (2004). Replication of two-photon-polymerized structures with extremely high aspect ratios and large overhangs. J. Phys. Chem. B *108*, 11256–11258. https://doi.org/10.1021/jp048525r.

77. Baldacchini, T., LaFratta, C.N., Farrer, R.A., Teich, M.C., Saleh, B.E.A., Naughton, M.J., and Fourkas, J.T. (2004). Acrylic-based resin with favorable properties for three-dimensional two-photon polymerization. J. Appl. Phys. *95*, 6072–6076. https://doi.org/10.1063/1.1728296.

78. Zandrini, T., Liaros, N., Jiang, L.J., Lu, Y.F., Fourkas, J.T., Osellame, R., and Baldacchini, T. (2019). Effect of the resin viscosity on the writing properties of two-photon polymerization. Opt. Mater. Express *9*, 2601. https://doi.org/10.1364/ome.9.002601.

79. Son, A.I., Opfermann, J.D., McCue, C., Ziobro, J., Abrahams, J.H., Jones, K., Morton, P.D., Ishii, S., Oluigbo, C., Krieger, A., et al. (2017). An implantable micro-caged device for direct local delivery of agents. Sci. Rep. *7*, 17624–17716. https://doi.org/10.1038/s41598-017-17912-y.

80. Berwind, M.F., Hashibon, A., Fromm, A., Gurr, M., Burmeister, F., and Eberl, C. (2017). Rapidly prototyping biocompatible surfaces with designed wetting properties via photolithography and plasma polymerization. Microfluid. Nanofluidics *21*, 144. https://doi.org/10.1007/s10404-017-1984-6.

81. Purtov, J., Rogin, P., Verch, A., Johansen, V.E., and Hensel, R. (2019). Nanopillar diffraction gratings by two-photon lithography. Nanomaterials *9*, 1495. https://doi.org/10.3390/nano9101495.

82. Guo, R., Li, Z., Jiang, Z., Yuan, D., Huang, W., and Xia, A. (2005). Log-pile photonic crystal fabricated by two-photon photopolymerization. J. Opt. Pure Appl. Opt. *7*, 396–399. https://doi.org/10.1088/1464-4258/7/8/008.

83. Yee, D.W., Schulz, M.D., Grubbs, R.H., and Greer, J.R. (2017). Functionalized 3d architected materials via thiol-michael addition and two-photon lithography. Adv. Mater. *29*, 1605293. https://doi.org/10.1002/adma.201605293.

84. Zakhurdaeva, A., Dietrich, P.I., Hölscher, H., Koos, C., Korvink, J.G., and Sharma, S. (2017). Custom-designed glassy carbon tips for atomic force microscopy. Micromachines *8*, 285–310. https://doi.org/10.3390/mi8090285.

85. Larramendy, F., Yoshida, S., Maier, D., Fekete, Z., Takeuchi, S., and Paul, O. (2019). 3D arrays of microcages by two-photon lithography for spatial organization of living cells. Lab Chip *19*, 875–884. https://doi.org/10.1039/c8lc01240g.

86. Gou, X., Zheng, M., Zhao, Y., Dong, X., Jin, F., Xing, J., and Duan, X. (2017). Mechanical property of PEG hydrogel and the 3D red blood cell microstructures fabricated by two-photon polymerization. Appl. Surf. Sci. *416*, 273–280. https://doi.org/10.1016/j.apsusc.2017.04.178.

87. Schwärzle, D., Hou, X., Prucker, O., and Rühe, J. (2017). Polymer microstructures through two-photon crosslinking. Adv. Mater. *29*, 1703469. https://doi.org/10.1002/adma.201703469.

88. Kufelt, O., El-Tamer, A., Sehring, C., Schlie-Wolter, S., and Chichkov, B.N. (2014). Hyaluronic acid based materials for scaffolding via two-photon polymerization. Biomacromolecules *15*, 650–659. https://doi.org/10.1021/bm401712q.

89. Maibohm, C., Silvestre, O.F., Borme, J., Sinou, M., Heggarty, K., and Nieder, J.B. (2020). Multi-beam two-photon polymerization for fast large area 3D periodic structure fabrication for bioapplications. Sci. Rep. *10*, 8740–8810. https://doi.org/10.1038/s41598-020-64955-9.

90. Marino, A., Ciofani, G., Filippeschi, C., Pellegrino, M., Pellegrini, M., Orsini, P., Pasqualetti, M., Mattoli, V., and Mazzolai, B. (2013). Two-photon polymerization of sub-micrometric patterned surfaces: investigation of cell-substrate interactions and improved differentiation of neuron-like cells. ACS Appl. Mater. Interfaces *5*, 13012–13021. https://doi.org/10.1021/am403895k.

91. Peng, Y., Jradi, S., Yang, X., Dupont, M., Hamie, F., Dinh, X.Q., Sun, X.W., Xu, T., and Bachelot, R. (2019). 3D photoluminescent nanostructures containing quantum dots fabricated by two-photon polymerization: influence of quantum dots on the spatial resolution of laser writing. Adv. Mater. Technol. *4*, 1800522–1800610. https://doi.org/10.1002/admt.201800522.

92. Marino, A., Barsotti, J., De Vito, G., Filippeschi, C., Mazzolai, B., Piazza, V., Labardi, M., Mattoli, V., and Ciofani, G.

(2015). Two-photon lithography of 3d nanocomposite piezoelectric scaffolds for cell stimulation. ACS Appl. Mater. Interfaces *7*, 25574–25579. https://doi.org/10.1021/acsami.5b08764.

93. Ovsianikov, A., Viertl, J., Chichkov, B., Oubaha, M., MacCraith, B., Sakellari, I., Giakoumaki, A., Gray, D., Vamvakaki, M., Farsari, M., and Fotakis, C. (2008). Ultra-low shrinkage hybrid photosensitive material for two-photon polymerization microfabrication. ACS Nano *2*, 2257–2262. https://doi.org/10.1021/nn800451w.

94. Klein, F., Richter, B., Striebel, T., Franz, C.M., von Freymann, G., Wegener, M., and Bastmeyer, M. (2011). Two-component polymer scaffolds for controlled three-dimensional cell culture. Adv. Mater. *23*, 1341–1345. https://doi.org/10.1002/adma.201004060.

95. Farsari, M., Vamvakaki, M., and Chichkov, B.N. (2010). Multiphoton polymerization of hybrid materials. J. Opt. *12*, 124001. https://doi.org/10.1088/2040-8978/12/12/124001.

96. Tudor, A., Delaney, C., Zhang, H., Thompson, A.J., Curto, V.F., Yang, G.Z., Higgins, M.J., Diamond, D., and Florea, L. (2018). Fabrication of soft, stimulus-responsive structures with sub-micron resolution via two-photon polymerization of poly(ionic liquid)s. Mater. Today *21*, 807–816. https://doi.org/10.1016/j.mattod.2018.07.017.

97. Correa, D.S., Tribuzi, V., Cardoso, M.R., Misoguti, L., and Mendonca, C.R. (2011). Selective excitation through tapered silica fibers of fluorescent two-photon polymerized structures. Appl. Phys. A *102*, 435–439. https://doi.org/10.1007/s00339-010-6165-3.

98. Mendonca, C.R., Baldacchini, T., Tayalia, P., and Mazur, E. (2007). Reversible birefringence in microstructures fabricated by two-photon absorption polymerization. J. Appl. Phys. *102*, 013109–13115. https://doi.org/10.1063/1.2752113.

99. Yoshida, H., Lee, C.H., Matsuhisa, Y., Fujii, A., and Ozaki, M. (2007). Bottom-up fabrication of photonic defect structures in cholesteric liquid crystals based on laser-assisted modification of the helix. Adv. Mater. *19*, 1187–1190. https://doi.org/10.1002/adma.200601753.

100. Kaneko, K., Sun, H.B., Duan, X.M., and Kawata, S. (2003). Two-photon photoreduction of metallic nanoparticle gratings in a polymer matrix. Appl. Phys. Lett. *83*, 1426–1428. https://doi.org/10.1063/1.1601302.

101. Focsan, M., Craciun, A.M., Astilean, S., and Baldeck, P.L. (2016). Two-photon fabrication of three-dimensional silver microstructures in microfluidic channels for volumetric surface-enhanced Raman scattering detection. Opt. Mater. Express *6*, 1587. https://doi.org/10.1364/ome.6.001587.

102. Son, Y., Lim, T.W., Yang, D.Y., Prabhakaran, P., Lee, K.S., Bosson, J., Stéphan, O., and Baldeck, P.L. (2010). Improvement of two-photon induced photoreduction by using a metal ion solution with a high concentration of silver ions. Int. J. Nanomanufacturing *6*, 219–230. https://doi.org/10.1504/IJNM.2010.034785.

103. Jaiswal, A., Rani, S., Singh, G.P., Hassan, M., Nasrin, A., Gomes, V.G., Saxena, S., and Shukla, S. (2021). Additive-free all-carbon composite: a two-photon material system for nanopatterning of fluorescent sub-wavelength structures. ACS Nano *15*, 14193–14206. https://doi.org/10.1021/acsnano.1c01083.

104. Jaiswal, A., Rani, S., Singh, G.P., Saxena, S., and Shukla, S. (2021). Two-photon lithography of fluorescence-encoded quick-read micro-code for anti-counterfeiting applications. J. Phys. Photonics *3*, 034021. https://doi.org/10.1088/2515-7647/ac0959.

105. Formanek, F., Takeyasu, N., Tanaka, T., Chiyoda, K., Ishikawa, A., and Kawata, S. (2006). Selective electroless plating to fabricate complex three-dimensional metallic micro/nanostructures. Appl. Phys. Lett. *88*, 083110. https://doi.org/10.1063/1.2178261.

106. Rill, M.S., Plet, C., Thiel, M., Staude, I., Von Freymann, G., Linden, S., and Wegener, M. (2008). Photonic metamaterials by direct laser writing and silver chemical vapor deposition. Nat. Mater. *7*, 543–546. https://doi.org/10.1038/nmat2197.

107. Xiong, W., Liu, Y., Jiang, L.J., Zhou, Y.S., Li, D.W., Jiang, L., Silvain, J.F., and Lu, Y.F. (2016). Laser-directed assembly of aligned carbon nanotubes in three dimensions for multifunctional device fabrication. Adv. Mater. *28*, 2002–2009. https://doi.org/10.1002/adma.201505516.

108. Zhou, W., Kuebler, S.M., Braun, K.L., Yu, T., Cammack, J.K., Ober, C.K., Perry, J.W., and Marder, S.R. (2002). An efficient two-photon-generated photoacid applied to positive-tone 3D microfabrication. Science *296*, 1106–1109. https://doi.org/10.1126/science.296.5570.1106.

109. Heiskanen, S., Geng, Z., Mastomäki, J., and Maasilta, I.J. (2020). Nanofabrication on 2d and 3d topography via positive-tone direct-write laser lithography. Adv. Eng. Mater. *22*, 1901290. https://doi.org/10.1002/adem.201901290.

110. Van der Velden, G., Fan, D., and Staufer, U. (2020). Fabrication of a microfluidic device by using two-photon lithography on a positive photoresist. Micro and Nano Engineering *7*, 100054. https://doi.org/10.1016/j.mne.2020.100054.

111. Tsutsumi, N., Hirota, J., Kinashi, K., and Sakai, W. (2017). Direct laser writing for micro-optical devices using a negative photoresist. Opt Express *25*, 31539–31551. https://doi.org/10.1364/oe.25.031539.

112. Cao, H.Z., Zheng, M.L., Dong, X.Z., Jin, F., Zhao, Z.S., and Duan, X.M. (2013). Two-photon nanolithography of positive photoresist thin film with ultrafast laser direct writing. Appl. Phys. Lett. *102*, 201108. https://doi.org/10.1063/1.4807678.

113. Tsutsumi, N., Fukuda, A., Nakamura, R., Kinashi, K., and Sakai, W. (2017). Fabrication of three-dimensional microstructures in positive photoresist through two-photon direct laser writing. Appl. Phys. A *123*, 553–557. https://doi.org/10.1007/s00339-017-1170-4.

114. Albota, M., Beljonne, D., Brédas, J.L., Ehrlich, J.E., Fu, J.Y., Heikal, A.A., Hess, S.E., Kogej, T., Levin, M.D., Marder, S.R., et al. (1998). Design of organic molecules with large two-photon absorption cross sections. Science *281*, 1653–1656. https://doi.org/10.1126/science.281.5383.1653.

115. Infuehr, R., Pucher, N., Heller, C., Lichtenegger, H., Liska, R., Schmidt, V., Kuna, L., Haase, A., and Stampfl, J. (2007). Functional polymers by two-photon 3D lithography. Appl. Surf. Sci. *254*, 836–840. https://doi.org/10.1016/j.apsusc.2007.08.011.

116. Xing, J.F., Dong, X.Z., Chen, W.Q., Duan, X.M., Takeyasu, N., Tanaka, T., and Kawata, S. (2007). Improving spatial resolution of two-photon microfabrication by using photoinitiator with high initiating efficiency. Appl. Phys. Lett. *90*, 131106–131114. https://doi.org/10.1063/1.2717532.

117. Zheng, Y.C., Zhao, Y.Y., Zheng, M.L., Chen, S.L., Liu, J., Jin, F., Dong, X.Z., Zhao, Z.S., and Duan, X.M. (2019). Cucurbit[7]uril-carbazole two-photon photoinitiators for the fabrication of biocompatible three-dimensional hydrogel scaffolds by laser direct writing in aqueous solutions. ACS Appl. Mater. Interfaces *11*, 1782–1789. https://doi.org/10.1021/acsami.8b15011.

118. Li, Z., Siklos, M., Pucher, N., Cicha, K., Ajami, A., Husinsky, W., Rosspeintner, A., Vauthey, E., Gescheidt, G., Stampfl, J., and Liska, R. (2011). Synthesis and structure-activity relationship of several aromatic ketone-based two-photon initiators. J. Polym. Sci. A. Polym. Chem. *49*, 3688–3699. https://doi.org/10.1002/pola.24806.

119. Mendonca, C.R., Correa, D.S., Baldacchini, T., Tayalia, P., and Mazur, E. (2008). Two-photon absorption spectrum of the photoinitiator Lucirin TPO-L. Appl. Phys. A *90*, 633–636. https://doi.org/10.1007/s00339-007-4367-0.

120. Xing, J.F., Chen, W.Q., Gu, J., Dong, X.Z., Takeyasu, N., Tanaka, T., Duan, X.M., and Kawata, S. (2007). Design of high efficiency for two-photon polymerization initiator: combination of radical stabilization and large two-photon cross-section achieved by N-benzyl 3,6-bis(phenylethynyl)carbazole derivatives. J. Mater. Chem. *17*, 1433–1438. https://doi.org/10.1039/b616792f.

121. Ohulchanskyy, T.Y., Donnelly, D.J., Detty, M.R., and Prasad, P.N. (2004). Heteroatom substitution induced changes in excited-state photophysics and singlet oxygen generation in chalcogenoxanthylium dyes: effect of sulfur and selenium substitutions. J. Phys. Chem. B *108*, 8668–8672. https://doi.org/10.1021/jp0370674.

122. Hua, Y., and Crivello, J.V. (2001). Development of polymeric photosensitizers

for photoinitiated cationic polymerization. Macromolecules *34*, 2488–2494. https://doi.org/10.1021/ma0018502.

123. Berberan-Santos, M.N., and Garcia, J.M.M. (1996). Unusually strong delayed fluorescence of C70. J. Am. Chem. Soc. *118*, 9391–9394. https://doi.org/10.1021/ja961782s.

124. He, J.H., and Mendoza, V.S. (1996). Synthesis and study of a novel hybrid UV photoinitiator: p-benzoyldiphenyliodonium hexafluorophosphate (PhCOPhI+PhPF6-). J. Polym. Sci. A. Polym. Chem. *34*, 2809–2816. https://doi.org/10.1002/(sici)1099-0518(2809)34:13<2809::aid-pola27>3.3.co;2-F.

125. He, J.H., and Zhang, J.C. (1999). Sensitized photolysis of diphenyliodonium cation through intra-ion-pair electron transfer - a novel near-UV photoinitiator: diphenyliodonium 9-acridinecarboxylate. J. Polym. Sci. Part A Polym. Chem. *37*, 4521–4527. https://doi.org/10.1002/(SICI)1099-0518(19991215)37:24<4521::AID-POLA8>3.0.CO;2-U.

126. Zhou, W., Liu, J., Wu, Z., and Wang, E. (1998). A novel pathway to photoinduced colour formation of colourless fluorane dye using iodonium salts as activators. J. Photochem. Photobiol. Chem. *112*, 173–178. https://doi.org/10.1016/S1010-6030(97)00259-1.

127. Zhou, W., and Wang, E. (1996). Photoinduced electron transfer in the ion pair compound (XTOn): influence of ionic association. J. Photochem. Photobiol. Chem. *96*, 25–29. https://doi.org/10.1016/1010-6030(95)04265-2.

128. Kim, S., Qiu, F., Kim, S., Ghanbari, A., Moon, C., Zhang, L., Nelson, B.J., and Choi, H. (2013). Fabrication and characterization of magnetic microrobots for three-dimensional cell culture and targeted transportation. Adv. Mater. *25*, 5863–5868. https://doi.org/10.1002/adma.201301484.

129. Costantino, S., Heinze, K.G., Martínez, O.E., De Koninck, P., and Wiseman, P.W. (2005). Two-photon fluorescent microlithography for live-cell imaging. Microsc. Res. Tech. *68*, 272–276. https://doi.org/10.1002/jemt.20247.

130. Jaiswal, A., Rani, S., Singh, G.P., Saxena, S., and Shukla, S. (2021). Two-photon lithography of subwavelength plasmonic microstructures in metal-polymer composite resin. Mater. Lett. *304*, 130642. https://doi.org/10.1016/j.matlet.2021.130642.

131. Ortiz-Huerta, F., Chen, L., Taverne, M., Hadden, J.P., Johnson, M., Ho, Y.L.D., and Rarity, J.G. (2018). Fabrication of hybrid Fabry-Pérot microcavity using two-photon lithography for single-photon sources. Opt Express *26*, 33245–33252. https://doi.org/10.1364/oe.26.033245.

132. Gittard, S.D., Ovsianikov, A., Akar, H., Chichkov, B., Monteiro-Riviere, N.A., Stafslien, S., Chisholm, B., Shin, C.C., Shih, C.M., Lin, S.J., et al. (2010). Two photon polymerization-micromolding of polyethylene glycol-gentamicin sulfate microneedles. Adv. Eng. Mater. *12*, B77–B82. https://doi.org/10.1002/adem.200980012.

133. Xiong, Z., Zheng, M.L., Dong, X.Z., Chen, W.Q., Jin, F., Zhao, Z.S., and Duan, X.M. (2011). Asymmetric microstructure of hydrogel: two-photon microfabrication and stimuli-responsive behavior. Soft Matter *7*, 10353–10359. https://doi.org/10.1039/c1sm06137b.